Magma addition and flux calculations of incrementally constructed magma chambers in continental margin arcs: Combined field, geochronologic, and thermal modeling studies

Scott R. Paterson[1], David Okaya[1], Valbone Memeti[1], Rita Economos[1], and Robert B. Miller[2]
[1]*Department of Earth Sciences, University of Southern California, Los Angeles, California 90089-0740, USA*
[2]*Department of Geology, San Jose State University, San Jose, California 95192-0102, USA*

ABSTRACT

Incrementally constructed magma systems have been recognized from studies of the resulting plutons for more than three decades. However, magma addition rates, fluxes, growth durations, sizes of increments, and sizes and durations of the resulting magma chambers have been difficult to ascertain, emphasizing the need for a better understanding of how magmatic systems evolve. Our results from studies of plutons and arc sections in the North American Cordillera indicate that a large range exists in all of these values. Although arc sections and individual plutons clearly have dramatic temporal changes in volumetric magma additions, true volumetric flux calculations are particularly difficult to determine. Thus, although subduction beneath arcs may have active durations of hundreds of millions of years, volumetrically most magmatism is emplaced during magmatic flare-ups of ~10–30 m.y. duration. Individual plutons and batholiths in these arcs can grow in <0.5 m.y. to 10 m.y. Pulse sizes moving through these magma plumbing systems vary from small dike-like to large diapir-like pulses, both of which may form from earlier amalgamation of poorly defined pulses. Our thermal modeling, using a range of incremental growth scenarios, concludes that focused incremental growth with greater than a certain volumetric flux results in magma chambers that are much larger than individual pulses but less than the size of the final batholith, and with hypersolidus durations of hundreds of thousands to millions of years. The volumetric magma flux and the spatial distribution of volumetric addition rates of magma, rather than size or shape of individual pulses, are the dominant controlling factors on growth scenarios and chamber sizes and durations.

INTRODUCTION

The evolution of continental margin orogens and their associated magmatic arcs involves the nonsteady state, coupled processes of subduction, orogeny, magmatism, exhumation, and erosion and/or redeposition. Recent studies have begun to examine the tempo of arcs driven in part by feedbacks between these processes (DeCelles et al., 2009). One well-established example of this tempo is the dramatic temporal change of volumetric addition rates of both magmatic (Ducea and Barton, 2007) and volcanic (de Silva and Gosnold, 2007) arcs from near zero to high values, the latter resulting in so-called magmatic surges or flare-ups, even though subduction and orogeny continued throughout both periods. For example, cyclic Mesozoic magmatism occurred in Cordilleran arcs in the Coast Ranges, British Columbia (Ducea, 2001; Gehrels et al., 2009); Cascades core, Washington (Paterson et al., 2004; Miller et al., 2009); Sierra Nevada, California (Tobisch et al., 1986; Busby-Spera, 1988; Saleeby, 1990; Dunne et al., 1998; Ducea, 2001; Saleeby et al., 2008); and the Transverse ranges, southern California (Barth et al., 1997, 2008) (Fig. 1).

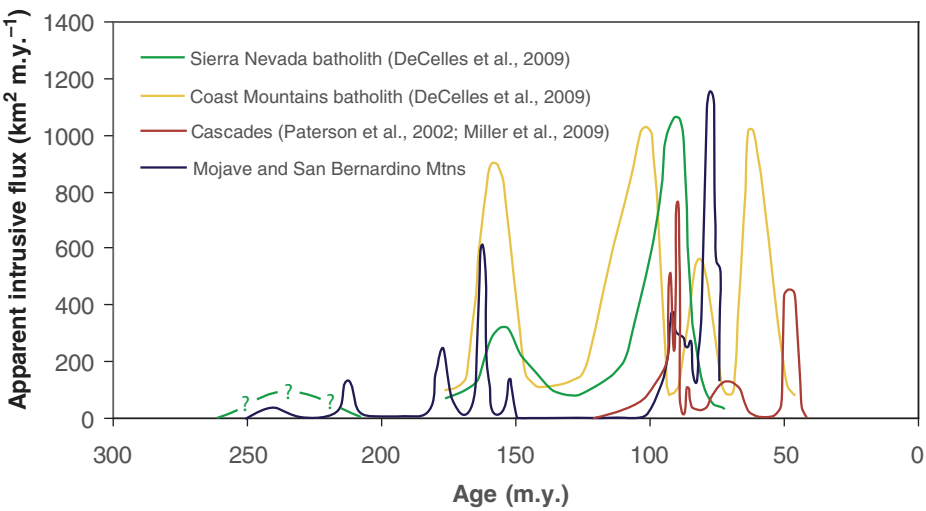

Figure 1. Diagram showing areal addition rates versus age for the Mesozoic Cordilleran arc in the Coast Mountains batholith; Cascades core, Washington; Sierra Nevada, California; and Transverse Ranges, Mojave Desert, southern California. Data are from A. Barth (2009, personal commun.), DeCelles et al. (2009), Ducea (2001), Gehrels et al. (2009), Miller et al. (2009), and Paterson et al. (2002). Note that magmatism in all settings is episodic, peak addition rates during surges of the same age are often similar in different parts of the arc, and spacings of peak flux events are similar in different parts of the arc. However, caution should be used in comparison of data from different regions since full information about areal extent examined, crustal depths, and calculations in cited data sources were often incomplete.

Geosphere; December 2011; v. 7; no. 6; p. 1439–1468; doi: 10.1130/GES00696.1; 19 figures; 3 appendix tables.

In this paper we combine our field and geochronologic studies of magma plumbing systems in arc crustal sections with our thermal modeling of incrementally grown, single magmatic systems to better understand some of the magmatic processes that affect arc tempos (Fig. 1). A central theme is a consideration of the difficult-to-calculate magma fluxes and resulting volume addition rates, and how best to compare these values in models with known boundary conditions to complex and much less well constrained natural magmatic systems preserved in arc crustal sections. Many authors infer fluxes from areal or volume addition rates of magma, but we treat these separately herein. The calculation of magmatic flux, as defined herein, also has been central in addressing two other important scientific goals. First, calculations of volcanic flux are commonly used as a predictive tool of the periodicity of volcanic systems (Wadge, 1981; Gamble et al., 2003; Adam et al., 2007; Hora et al., 2007) and to infer the behavior of subvolcanic magma chambers (Crisp, 1984; Bacon and Lanphere, 2006; Scandone et al., 2007). Second, estimates of arc-scale magma addition rates are applied to questions of crustal genesis (Ducea, 2002), the mass balance of felsic plutonism, and the required resulting restitic component (Ducea, 2001). Between the fine scale of single volcanic centers and the very broad scale of entire arc systems, calculations of true volumetric addition rates and inferred magmatic fluxes are fraught with challenges. However, the scale of magma flux for an individual pulse, a pluton, or a suite of plutons is critical to our understanding of the evolution of incrementally grown systems (e.g., Saleeby et al., 2008), and assumptions about the scale of magma flux are inherent in batholith construction models.

A consideration of Figure 1 raises several critical issues regarding magmatic addition rates and fluxes at various scales (see following definitions). Figure 1 is compiled from different publications using different definitions, and thus we have tried to prepare data sets for comparison by converting to areal addition rates, called apparent areal fluxes in the cited papers, and thus emphasize that this plot does not show volumetric magmatic fluxes. There are a number of interesting components that warrant further discussion, including: (1) the ages of plutons and thus ages of areal addition rate highs and lows; (2) the spacing between magmatic surges; (3) the heights of area addition rate maxima; and (4) the area under the curves and thus total area (or volume in three dimensions) of magmatism represented by each peak. Not all of these four aspects of Figure 1 are as equally well constrained. Most robust are the ages of plutons, and thus ages of peaks and lulls, because of the increasingly widespread U-Pb zircon data available. It is interesting that in this Cordilleran Mesozoic arc the spacing between surges or lulls is ~70 m.y. in the Triassic and Jurassic, but decreases to more complicated ~20 m.y. spacing in the Cretaceous. Also note that the peaks tend to occur at approximately similar ages, even though these data come from arc segments examined over distances of thousands of kilometers apart.

The peaks and valleys of the curves are less well constrained and will probably shift somewhat as more plutons are examined. These are very dependent on whether results are all normalized to a certain unit area (km^2), what arc depth is examined, and how one relates magma fluxes and volumetric addition rates in active arcs to frozen plutons (a topic addressed in detail herein). These estimates are also dependent on exposure: for example, bedrock exposure in the high Sierras is commonly 80%, whereas in the Joshua Tree (Transverse Ranges) section of the arc bedrock exposure is only ~30%–50%. However, a fairly robust pattern of episodic and increasing volumes of magmatism from the Triassic to Jurassic and particularly in the Cretaceous is indicated for this arc.

It is also intriguing to note that the heights of areal addition rates during magmatic surges increase with decreasing age and, for any given age, are fairly consistent from one part of this Cordilleran arc to another. True areal addition rates are difficult to determine precisely but apparently vary from ~150 (Triassic) to 800 (Jurassic) to 1000 (Cretaceous) per arc length (km^2/km m.y.$^{-1}$) during magmatic surges to near zero during magmatic lulls. This dramatic variation raises a number of interesting questions, including what generates the different volumes of magmatism, how the crust responds to accommodate both high and low volumetric addition events, and the degree to which volumetric fluxes in individual magma plumbing systems change through time (and thus potentially have their own tempo).

If one considers individual magma plumbing systems, sheeted dike and sill complexes are fairly clear examples of plutonic bodies constructed by magma pulsing, although it is not always clear how far traveled or chemically distinct each dike or sill is. Different pulses of magma also have been recognized in larger plutons and batholiths for many decades. Recognition of these pulses has been used to argue that even large plutonic bodies may incrementally grow by the addition of a few to numerous pulses of magma and that this growth may be complex (e.g., Pitcher and Berger, 1972; Hardee, 1982; Hutton, 1982, 1992; Lagarde et al., 1990; Paterson and Vernon, 1995; McNulty et al., 1996; Vigneresse and Bouchez, 1997; Paterson and Miller, 1998; Wiebe and Collins, 1998; Johnson et al., 1999; Miller and Paterson, 2001a). Continued interest in incremental growth of large plutonic bodies (e.g., Coleman et al., 2004; Matzel et al., 2005, 2006a; Walker et al., 2007) has been largely driven by studies of volcanic systems (e.g., Bacon and Lowenstern, 2005; Lipman, 2007; Bindeman et al., 2008), increasingly precise U-Pb thermal ionization mass spectrometry (TIMS) zircon dating of multiple single grains (e.g., Brown and Fletcher, 1999; Mattinson, 2005; Charlier et al., 2005; Matzel et al., 2006b; Miller et al., 2007; Memeti et al., 2010), and single mineral geochemical studies (Davidson et al., 1998, 2005, 2007; Christensen et al., 1995; Hoskin et al., 1998; Costa et al., 2003; Barbey et al., 2005; Ramos and Reid, 2005; Gagnevin et al., 2005; Wallace and Bergantz, 2005; Morgan et al., 2007), studies that increasingly conclude that magma batches with distinct histories occur at all crustal levels in magma plumbing systems and range from <10 m^3 to >1000 km^3. These studies further show that crystals in these pulses often preserve complex geochemical histories and a range of ages indicating dramatic crystal and melt(?) exchange between pulses.

Recent studies have particularly raised the issue of the degree to which large plutonic bodies and batholiths ever consisted of large magma chambers (e.g., cf. Glazner et al., 2004, and Lipman, 2007). If large batholiths were constructed from smaller magma batches, the degree to which a large magma chamber formed (probably always smaller than the final batholith, but potentially significantly bigger than individual pulses) ultimately depends on the initial conditions of batholith formation plus the volumetric flux of magma into the growing batholith. Thermal modeling of incrementally grown magma systems documents that steady-state regions of crystal mushes can grow to large sizes if spatial focusing of magma occurs and the volumetric flux is high relative to conductive cooling (Sleep, 1975, 1991; Wilson et al., 1988; Hanson and Glazner, 1995; Yoshinobu et al., 1998; Paterson et al., 2007).

We examine these issues at scales ranging from single plutons to large sections of arcs. We consider evidence for (1) size of pulses or growth increments; (2) rates of pulsing, periodicity, and both magma addition rates and volumetric fluxes; (3) location of pulse amalgamation; and (4) size and duration of resulting magma chambers. We combine field and geochronologic studies and use these results as constraints for finite difference thermal modeling of incrementally grown systems. We return to an

evaluation of the challenges of estimating volumetric fluxes and choosing between the diverse incremental growth scenarios introduced here.

DEFINITIONS

A clearly defined set of terms is needed when considering topics of incremental growth. Typical volume flux calculations, such as those used to measure stream flow or fluid flow through porous media (Darcy's law), are defined as a volume passing through a designated area over a period of time (e.g., $km^3/km^2/yr = m/s$) and this is how we use volumetric magmatic flux in this paper (Appendix Table A1). We retain volumetric in this term to distinguish from fluxes looking at mass or heat or other possible flux measurements. We also define the terms total added volume (km^3) as the volumetric amount of material added and volumetric addition rate (km^3/yr) as the total added volume per time (Appendix Table A1), both of which are not normalized by measurement area but are often more easily determined measurements when dealing with natural systems (discussed herein). We note that our term of volumetric addition rate is referred to as a magmatic flux by some, but does not have traditional flux units ($km^3/km^2/yr$). To remove debates about the three-dimensional (3-D) shapes of plutons, often due to lack of direct knowledge, and because little information is preserved in paleoarcs about the actual volumetric magmatic flux, authors typically use more readily determined areal measurements to determine apparent areal fluxes (km^2/yr). Sometimes areal or volumetric addition rates are normalized to arc segments, the latter called arc length flux or Armstrong unit ($km^3/yr/arc\text{-}km$). These are not true flux calculations, and we thus use the terms areal or volume addition rate per arc length to distinguish them from volumetric flux in this paper. Appendix Table A1 summarizes some of the different uses of these terms.

All of these different measurements have direct relationships to one another, as graphically shown in Figure 2. Relating magma pulse size and number of pulses emplaced per unit time defines volume addition rates (Fig. 2A), and volume addition rates and areal dimensions of magma feeder zones can be related to volumetric fluxes (Fig. 2B). Unfortunately, as discussed herein, these different values are often difficult to impossible to determine in natural systems. We use Figure 2 to explore where values for natural systems may plot on these graphs (see Discussion).

Prior to evaluating incremental growth in natural systems, it also is important to consider what a now-solid pluton represents. There are two end members, and a spectrum of intermediate possibilities, for how we can view plutonic bodies (Fig. 3). One end member is that a plutonic body reflects a former single, connected, and fairly closed batch of magma (but still potentially constructed earlier by more than one pulse) that froze while rising through the crust, such as one might view a diapir or dike disconnected from its sources (Fig. 3A). Another view is that plutonic bodies are frozen parts of a former complex magma transfer zone or plumbing system that may be quite extensive, evolve over time, be utilized during a number of magma ascent events, remobilize and recycle material from older pulses or host rock, and thus remain open systems for an extended duration (Figs. 3C, 3D). Many intermediate examples are possible: (1) a fairly isolated batch of magma rising up a previously used magma pathway (Fig. 3D); (2) variable volumetric fluxes in, or reuse of, dike channels (Fig. 3B); and (3) the rising tail of a diapir resulting in continued addition to a stalled diapir head (Fig. 3B). Other processes that complicate the growth of magma chambers (plutons) may occur in any of these scenarios, such as (1) localized differential movement of magma entirely within an existing batch of magma; (2) magma pulses moving back down the magma pathway during rise of other pulses; (3) pulses entirely lost from the plutonic system through volcanic eruption; (4) reheating of crystal mush zones resulting in

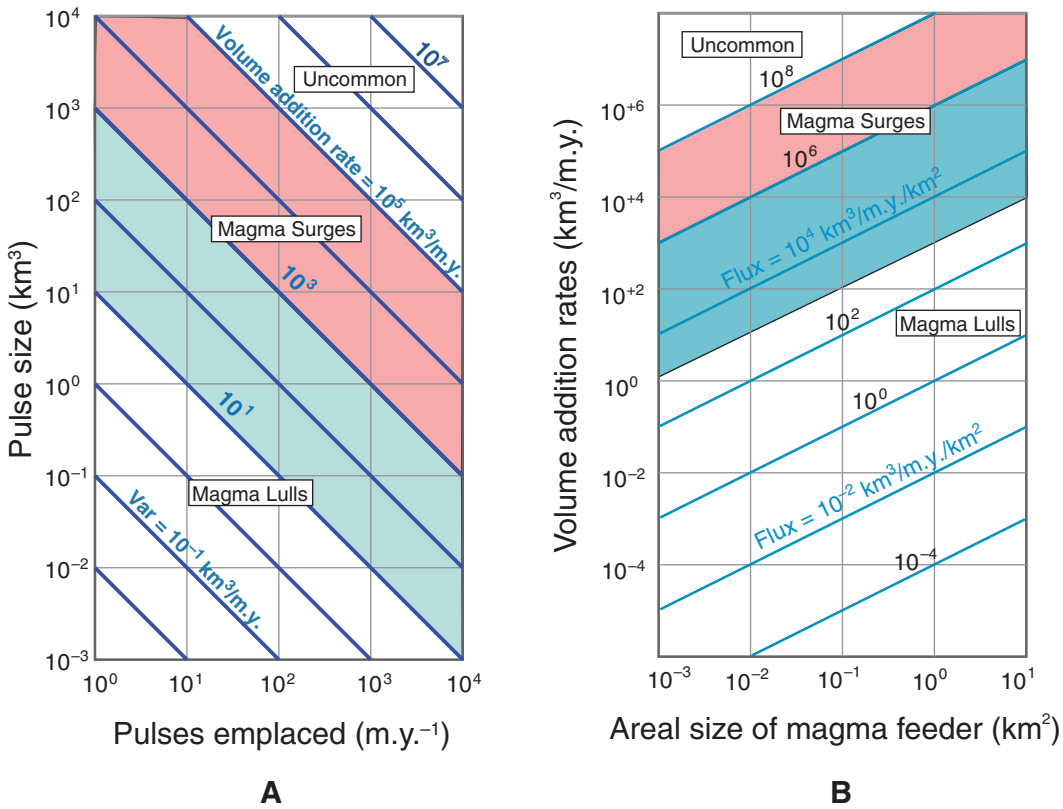

Figure 2. (A) Magma pulse size, frequency of pulse emplacement, and volume addition rates (blue lines). (B) Magma addition rates, areal dimensions of magma feeder zones, and volumetric fluxes (blue lines). Pink areas show values common in natural systems during magmatic surges and in our thermal models in which large addition and/or flux rates are used. Light blue regions are typical values for regional background magmatism in arcs and for scenarios with small pulse sizes in our thermal models. Values in the uncolored upper corners of these plots are not common in magmatic systems, although they may be appropriate during short duration volcanic eruptions. Values in the uncolored region in the lower left of the diagrams are appropriate for magmatic lulls.

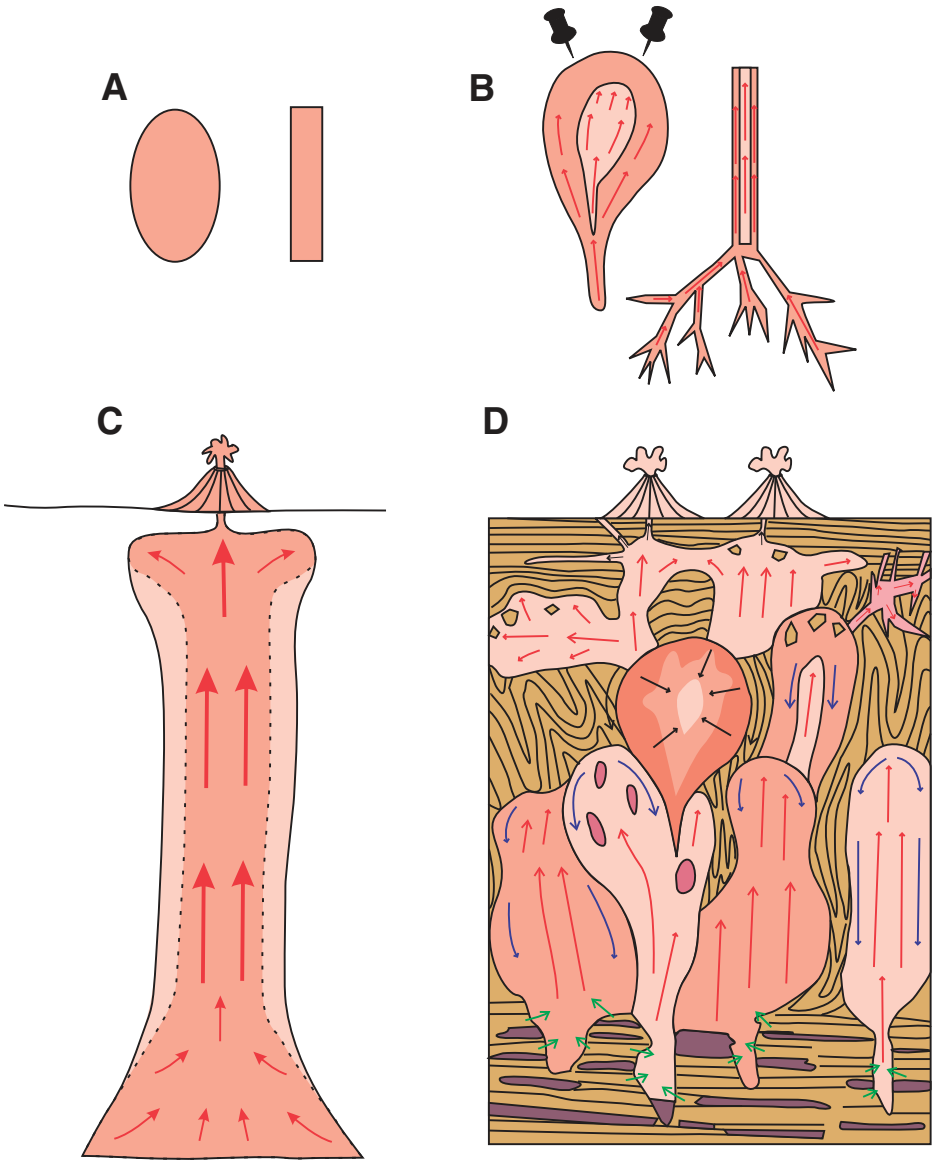

Figure 3. Examples showing what plutonic bodies possibly represent. (A) A single connected and fairly closed batch of magma (diapir or dike) that has been disconnected from its source. (B) The rising tail of a diapir resulting in continued addition to a stalled diapir head or a dike that continues to get fed from the source. (C) A continuous, preheated magma pathway that is connected to its source at depth and to volcanoes at the surface, forming an open magma plumbing system. (D) A more realistic magma plumbing system that forms an open system as in C, but is also influenced and characterized by local complications such as downward flow within plutons (blue arrows); mixing, mingling, and fractionation processes; introduction of host materials through leucosomatic melts (green arrows); and stoped blocks, diking, and surface uplift through laccolith formation.

their reactivation and continued movement in a magma channel; and (5) internal differentiation processes resulting in compositional and structural diversity, which might resemble pulse-like bodies (Fig. 3D).

Because all of these scenarios are possible, we are faced with a number of challenging questions, such as whether magma more commonly ascends during continuous or pulse-like flow. If the latter, can we recognize distinct magma pulses and whether these pulses were assembled in situ or elsewhere and then moved en masse to their final location? Can we recognize a batch of magma with distinct characteristics that formed locally versus another that is truly far traveled? How is it best to determine volumetric fluxes versus areal or volumetric addition rates in these frozen magmatic systems? Many of these questions are analogous to tectonic questions faced during studies of suspect terranes, in which adjacent terranes (magma batches), with different characteristics, may or may not be related. As with suspect terranes, it is clearly important to establish useful criteria for distinguishing pulses formed during the different scenarios. We return to this topic after first evaluating natural systems.

GEOLOGIC DESCRIPTIONS OF DIFFERENT ARCS

We summarize our studies of continental margin arcs in two different areas (Fig. 4): (1) the Mesozoic central Sierra Nevada Batholith, California, in which we focus on upper crustal plutons, particularly recent work on the Tuolumne batholith (Figs. 5 and 6), but have data available through published studies from near surface to ~35 km depths; and (2) the Cascades core, Washington (Figs. 7 and 8), consisting of a composite crustal section exposing Mesozoic and early Tertiary magmatic systems from ~5–35 km; we have completed extensive studies on many plutons at all crustal levels here (Miller et al., 2009). We do not discuss in detail, but are influenced by our work in progress on two newly recognized crustal sections, (1) the Paleozoic Gobi-Tienshan intrusive complex, Mongolia, and overlying volcanics (0–15 km depths; Economos, 2009) and (2) a 0–20 km tilted section in Joshua Tree National Park, Transverse Ranges, California (Needy et al., 2009). Tentative crustal columns developed from these four areas are shown in Figure 9.

Sierra Nevada Batholith

The Sierra Nevada Batholith is part of the North American Cordilleran magmatic arc, which formed as a result of Mesozoic subduction of the Farallon plate beneath the North American plate (Fig. 4). It is composed of ~0.7 × 10^6 km^3 (Ducea, 2001) granodioritic to granitic magmas, mainly calc-alkaline magnetite series, that formed a batholith ~30–35 km thick (now 25–30 km; Saleeby et al., 2008) underlain by a thick crustal residue (Ducea, 2001). U-Pb zircon ages and compilation of the NAVDAT (Western North American Volcanic and Intrusive Rock Database; www.unc.edu/~breckj/navdat.htm) reveal that although the arc was active between ca. 240 Ma and 80 Ma (Saleeby et al., 2008; Ducea, 2001), magmatism occurred episodically in magma flare-ups (Fig. 1), which were separated by 25–70 m.y. long magmatic lulls (DeCelles et al., 2009). Significant flare-ups took place during the Late Jurassic (160–150 Ma) and

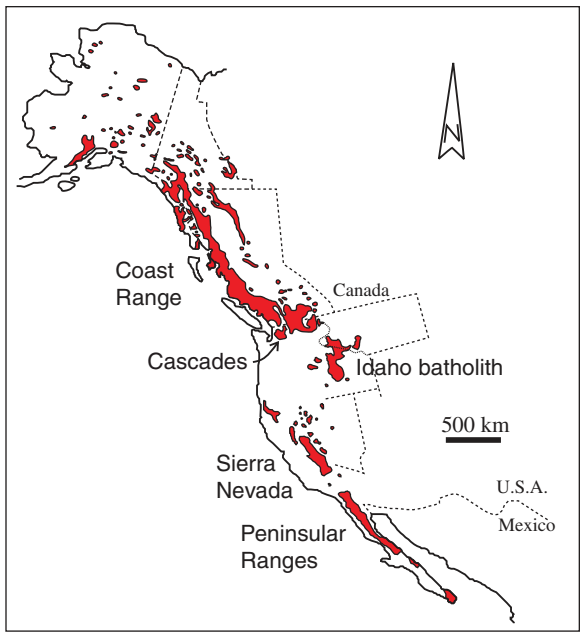

Figure 4. Mesozoic and Paleogene arc plutons (red) in the western North American Cordillera from northernmost Alaska to southern Baja California (redrafted by Erwin Melis after Anderson, 1990).

particularly the Late Cretaceous (100–85 Ma; Coleman and Glazner, 1997; Ducea, 2001). Barth et al. (2008) emphasized Permian–Triassic and Middle Jurassic (180–165 Ma) episodes of voluminous magmatism, the latter being particularly widespread in the central and eastern Transverse Ranges, southern California.

Tuolumne Batholith

One of the most studied large intrusive bodies in the Sierra Nevada is the Tuolumne batholith (TB). This 1100 km^2 batholith is one of 4 intrusive suites of similar composition and age exposed along the eastern Sierra Nevada crest (Fig. 5, inset; Bateman, 1992; Coleman and Glazner, 1997). The TB intruded during the Late Cretaceous magma flare-up (Ducea, 2001) and crystallized at ~2–3 kbar (Ague and Brimhall, 1988; Gray, 2003; Memeti et al., 2009). The TB intruded into early Paleozoic metasediments (western) and greenschist facies metasedimentary, metavolcanic (eastern), and plutonic rocks related to the Mesozoic Sierran arc (Huber et al., 1989).

The TB (Figs. 5 and 6) is composed of three main, partially nested, intrusive units (Bateman and Chappell, 1979) that in general become younger and more felsic toward the center and northward (Memeti et al., 2010), and scattered leucogranite bodies: (1) the outer 95–92 Ma Kuna Crest granodiorite to the east and its equivalents along the western and southern margins (tonalites of Glen Aulin and Glacier Point, granodiorite of Grayling Lake), which are mostly fine- to medium-grained tonalites and granodiorites (Kistler and Fleck, 1994; Coleman et al., 2004; Memeti et al., 2010); (2) the 92–88 Ma Half Dome Granodiorite, subdivided into an outer equigranular granodiorite and the inner K-feldspar porphyritic phase (Kistler and Fleck, 1994; Coleman et al., 2004; Matzel et al., 2005, 2006b; Memeti et al., 2010); (3) the 88–85 Ma medium-grained Cathedral Peak Granodiorite with K-feldspar phenocrysts as large as 12 cm and 1 cm quartz pools (Kistler and Fleck, 1994; Coleman et al., 2004; Matzel et al., 2005, 2006b; Memeti et al., 2010); and (4) the geographically centrally located, ca. 87.5 Ma Johnson Granite Porphyry and similar bodies farther north, consisting of fine-grained leucogranite with local K-feldspar megacrysts that are likely to be antecrysts from the Cathedral Peak unit (Fig. 5; Bateman and Chappell, 1979; Titus et al., 2005; Bracciali et al., 2008). Contacts between the above units are generally steep and vary from knife sharp (Fig. 6A) to gradational over hundreds of meters with hybrid phases within the latter zones (e.g., Bateman and Chappell, 1979; Žák and Paterson, 2005; Memeti et al., 2010; Fig. 5). These contacts are overprinted by magmatic fabrics that form late during the hypersolidus evolution of the batholith (Žák et al., 2007). Subtle, transitional contacts are recognized due to gradational changes in grain size, texture, and/or composition. The hybrid phases contain typical characteristics of both adjacent units; this is also reflected in element geochemistry (Memeti et al., 2007). Microgranitoid enclaves are abundant in the two marginal TB units, where they form dispersed enclaves, enclave swarms, and enclave accumulations of a variety of compositions (Memeti and Paterson, 2008). Locally, enclaves mix and mingle with their host magma (Fig. 6B). Enclaves in the Cathedral Peak granite are less common and mostly absent in the Johnson Peak granite. In these units various crystal accumulations occur in the form of K-feldspar megacryst pipes, diapirs, and irregular masses. Along external and internal pluton contacts, but also within single TB units, complex schlieren zones defining a variety of magmatic structures such as layered mafic schlieren, tubes, troughs, enclave swarms, pipes, and small diapirs are preserved (Figs. 6C, 6D; Žák and Paterson, 2005; Paterson et al., 2008; Paterson, 2009). Mafic schlieren layers are zones that are characterized by the higher abundance of mafic minerals and high-density accessories (e.g., zircon, sphene). Studies on schlieren structures such as troughs and tubes, where mixed populations of minerals derived from different TB units were found, are interpreted to have formed due to magmatic gravity flows (Solgadi and Sawyer, 2008) and local flow instabilities in magma mushes (Paterson, 2009). Host-rock xenoliths (stoped blocks) are mostly found at the margin of the TB, and decrease in abundance toward the center, although cognate inclusions (stoped blocks of earlier pulses) can be found in all units. Most geochemistry studies, which looked at element and isotope distributions of the main TB units, argue for mixing as the dominant internal magma chamber process causing the compositional variation in the TB (Kistler et al., 1986; Burgess and Miller, 2008; Memeti et al., 2007). Fractionation crystallization patterns are preserved in some domains, such as the magmatic lobes or in individual minerals, and indicate that fractionation crystallization is an important magma chamber process as well, but is masked by the mixing processes in the central chamber or chambers (Memeti et al., 2007, 2010; Burgess and Miller, 2008). Mixing as an important process responsible for compositional variations in the TB has also been supported by precise U-Pb chemical abrasion–TIMS zircon geochronology studies, which suggests that antecrystic zircons in an earlier-formed magma mush are recycled into younger pulses intruding into the central and/or younger parts of the batholith (Miller et al., 2007; Matzel et al., 2005; Memeti et al., 2010).

Growth Models for the TB

Several models have been proposed to explain the construction and compositional evolution of the TB. Bateman and Chappell (1979), using element geochemistry, suggested that the TB formed by crystal-liquid fractionation of one single batholith-sized pulse. Isotopic data from Kistler et al. (1986) disproved this idea, and suggested instead that mixing of different mantle-

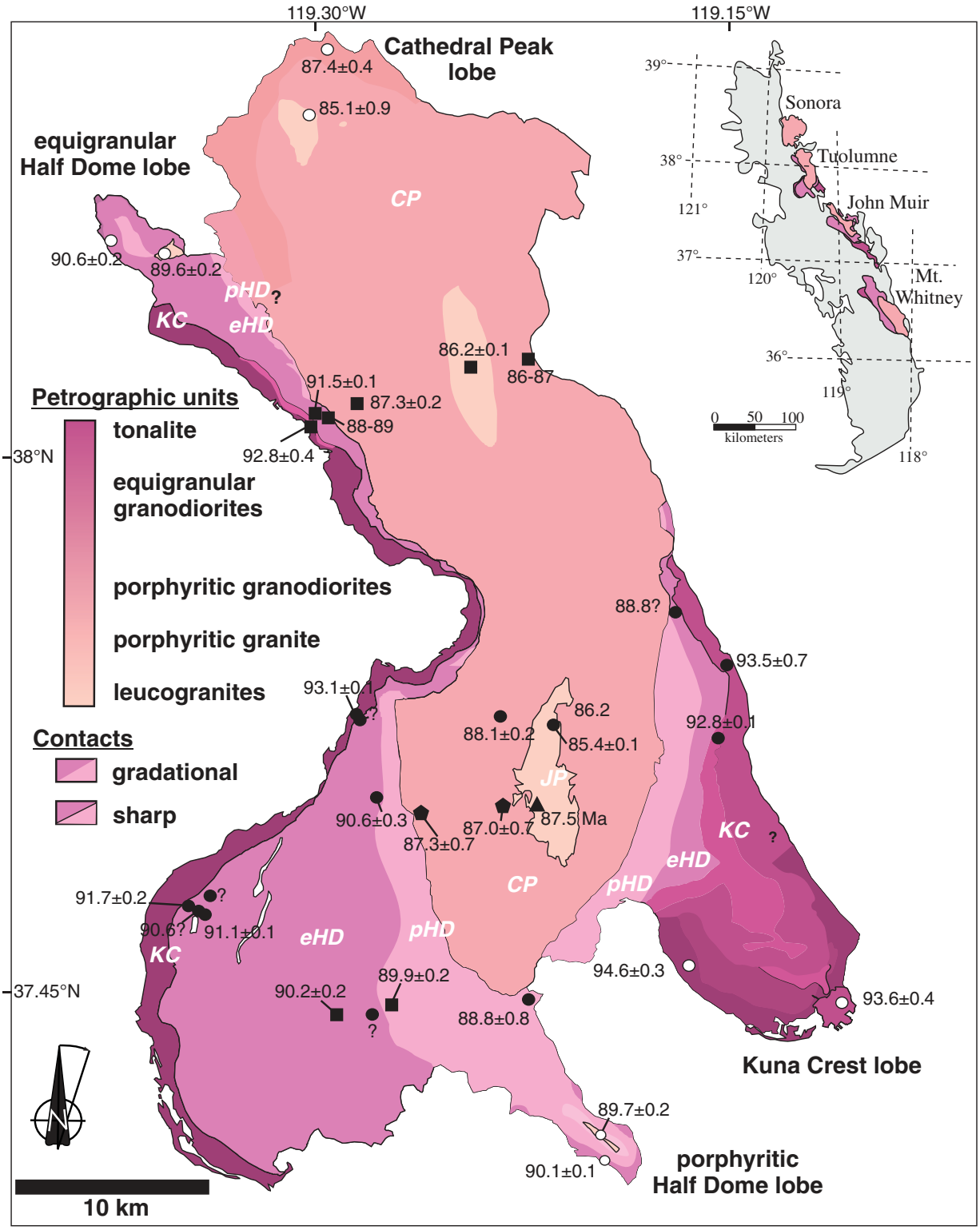

Figure 5. Simplified geologic map of the Tuolumne batholith (modified from Huber et al., 1989) with detailed lobe mapping (from Memeti et al., 2010). Inset map shows Mesozoic Sierra Nevada magmatic arc with major Cretaceous intrusive suites (redrafted after Kistler and Fleck, 1994). Black circles—U-Pb zircon ages of Coleman and Glazner (1997) and Coleman et al. (2004); squares—zircon ages of Matzel et al. (2005, 2006b); pentagons—zircon ages of Burgess and Miller (2008); black triangle—Johnson Peak (JP) porphyry age of Bracciali et al. (2008); white circles—ages of Memeti et al. (2010). KC—Kuna Crest granodiorite, eHD—equigranular Half Dome Granodiorite, pHD—porphyritic Half Dome Granodiorite, CP—Cathedral Peak Granodiorite and/or granite.

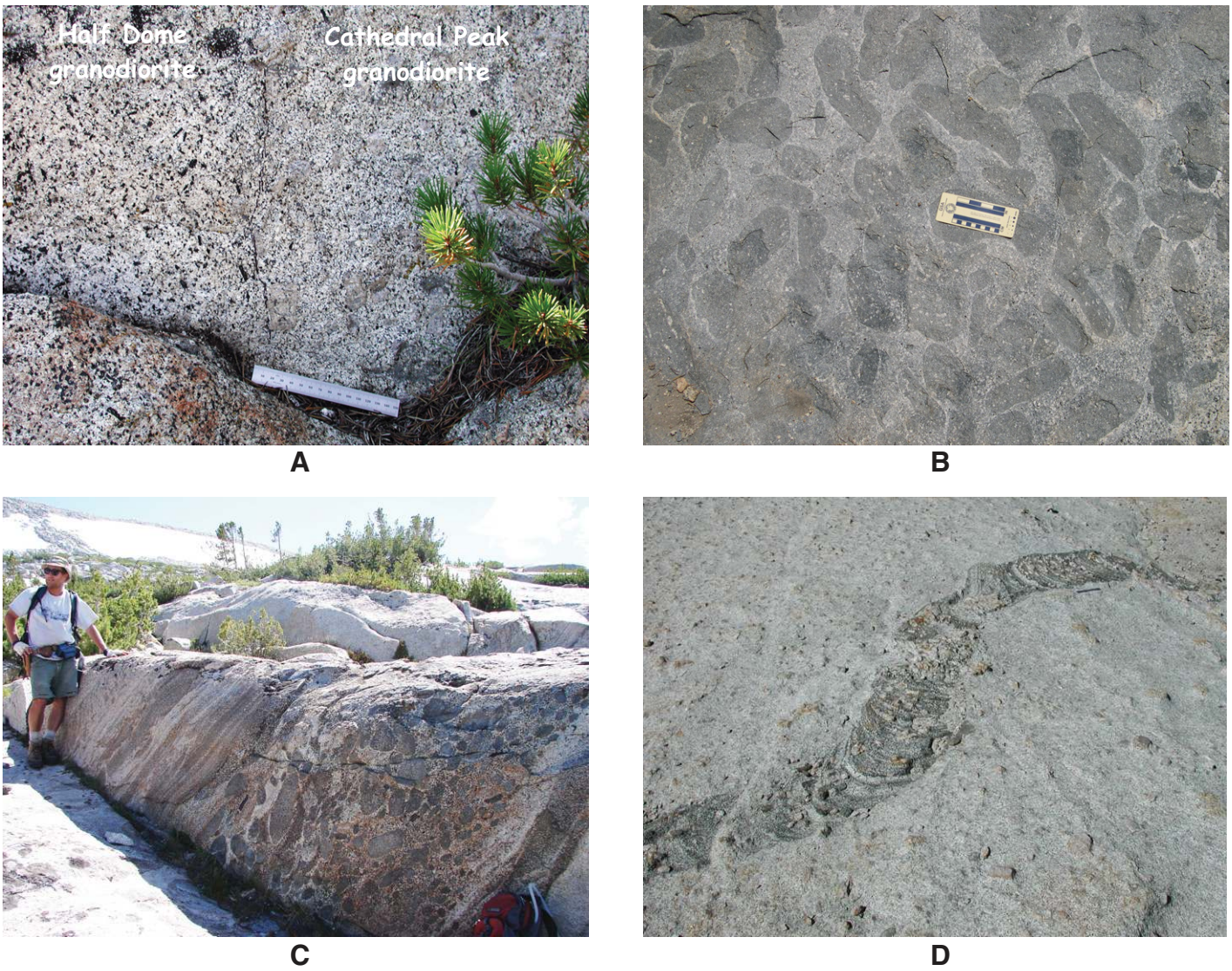

Figure 6. Outcrop photos from the Tuolumne batholith, Sierra Nevada. (A) Sharp and simple contact between the porphyritic Half Dome Granodiorite and the Cathedral Peak Granodiorite. Mineral fabrics (alignment of dark minerals) are parallel and at a high angle to the contact. (B) Mingling and mixing of granodiorite and quartz-diorite magmas in the Kuna Crest lobe. (C) Complex schlieren and mingling zone in equigranular Half Dome Granodiorite, including mafic and felsic schlieren layers, enclave swarms, and ridge-and-pillar structures (Mammoth Peak, eastern Tuolumne batholith). (D) Schlieren tube with steep axis formed during local magma flow in Cathedral Peak Granodiorite. Image in photo is ~3 m wide.

derived basalts and crustal granitic melts formed the compositional diversity in the TB. Four contrasting chamber growth models have been proposed recently for the TB. (1) The incremental intrusion of a few internally fractionating nested units formed a large magma chamber and mixed and/or mingled along margins between TB units (Paterson and Vernon, 1995; Žák and Paterson, 2005). We would accept that smaller, compositionally similar pulses may have fed these four separate TB units, but they then amalgamated to form larger magma bodies (Memeti et al., 2010). (2) Gray et al. (2008), on the basis of the geochemistry of the southwestern TB, suggested that mixing of magmas from different sources is an important internal process in creating the compositional diversity in the TB. They conclude that internal contacts and the textural variation of the different TB units at the emplacement level may be interpreted as one petrological continuum formed by the thermal evolution of the system rather than defining distinct intrusive events. (3) The incremental assembly of the TB occurred by the intrusion of numerous dikes over ~10 m.y., during which time each dike cooled enough to prevent significant chemical exchange with subsequent dikes (Coleman et al., 2004). (4) Stacked, downward-building laccoliths were constructed by a syntaxial crack-seal mechanism, whereby the laccolithic layers were folded and in places entirely solid during continued growth (Tikoff and Teyssier, 1994; Bartley et al., 2008). If the latter two models are correct, a large magma chamber never existed during the evolution of the TB, the four main units are only superficially homogeneous, and the models also imply that little fractionation or mixing occurred at the emplacement site (Coleman, 2005).

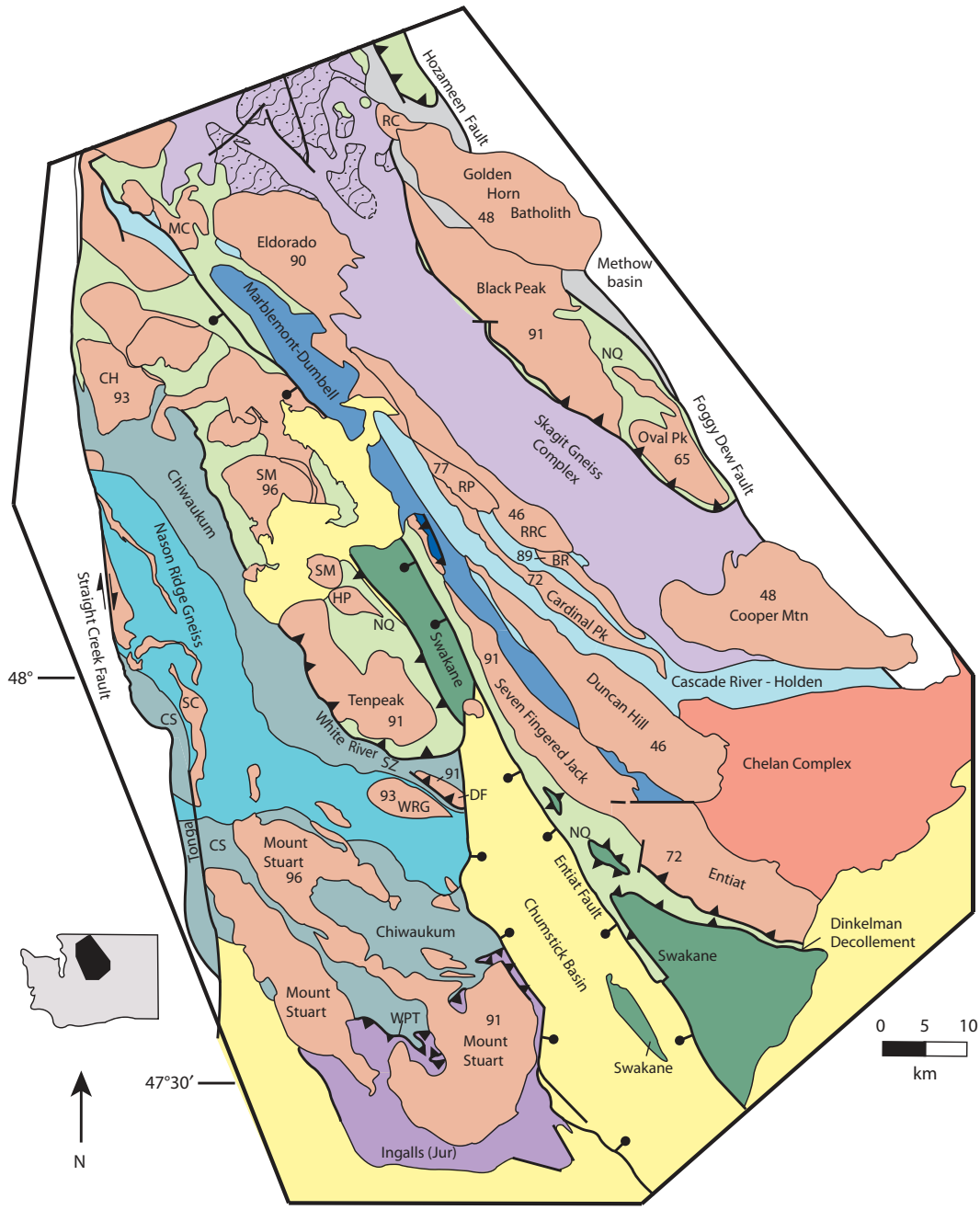

Figure 7. Simplified geologic map emphasizing the Cascades core. Plutons are colored pink and numbers are crystallization ages; BR—Bearcat Ridge Orthogneiss; CH—Chaval pluton; CS—Chiwaukum Schist; DF—Dirtyface pluton; HP—High Pass pluton; MC—Marble Creek pluton; NQ—Napeequa unit; RRC—Railroad Creek pluton; RP—Riddle Peaks pluton; SC—Sloan Creek plutons; SM—Sulphur Mountain pluton; WPT—Windy Pass thrust; WRG—Wenatchee Ridge Gneiss. The Methow basin and Northwest Cascades system west of the Straight Creek Fault are shown with the same color, emphasizing their Cretaceous and/or older age and low-grade to nonmetamorphic rocks. Inset shows Washington State and location of the geologic map.

Magma Chamber Extent, Pulse Size, and Pulsing

All recently proposed models for the TB and similar plutons elsewhere agree that plutonic bodies like the TB are probably constructed by the emplacement of incremental magma pulses rather than a single pulse. However, views diverge about the pulse sizes or increments feeding TB-like magma bodies and the maximum magma chamber size that formed. The pulse size suggested for the TB varies in the different models from small dikes that may feed and/or form laccolith- and/or lopolith-type bodies (Bartley et al., 2008), to the size of the four magmatic lobes, which can be as large as 10–60 km^2 (and likely 100–600 km^3; Oliver et al., 1988; Bateman, 1992; Memeti et al., 2010), or as large as the extent of an individual unit or lithodeme in the TB (Paterson and Vernon, 1995; Žák and Paterson, 2005). The stacked laccolith model (model 4) requires that if plutons grow "in increments that are substantially smaller than the ultimate dimensions of the pluton, the increments must be added episodically at rates several orders of magnitude faster than the long-term average growth rate." This implies that "the active magma body at any point of time may be small compared to the pluton that contains it, and a pluton even may be entirely solid at times during its growth" (Bartley et al., 2008, p. 383). Our evaluation of all field and analytic studies of the TB accumulated over the years and attempts to test the models suggest to us that some variation of the first model, in which large chambers existed and magmatic processes such as fractionation crystallization, mixing, and recycling took place at the emplacement level, but with some components of the Gray et al. (2008) model, still best describes the incremental growth of

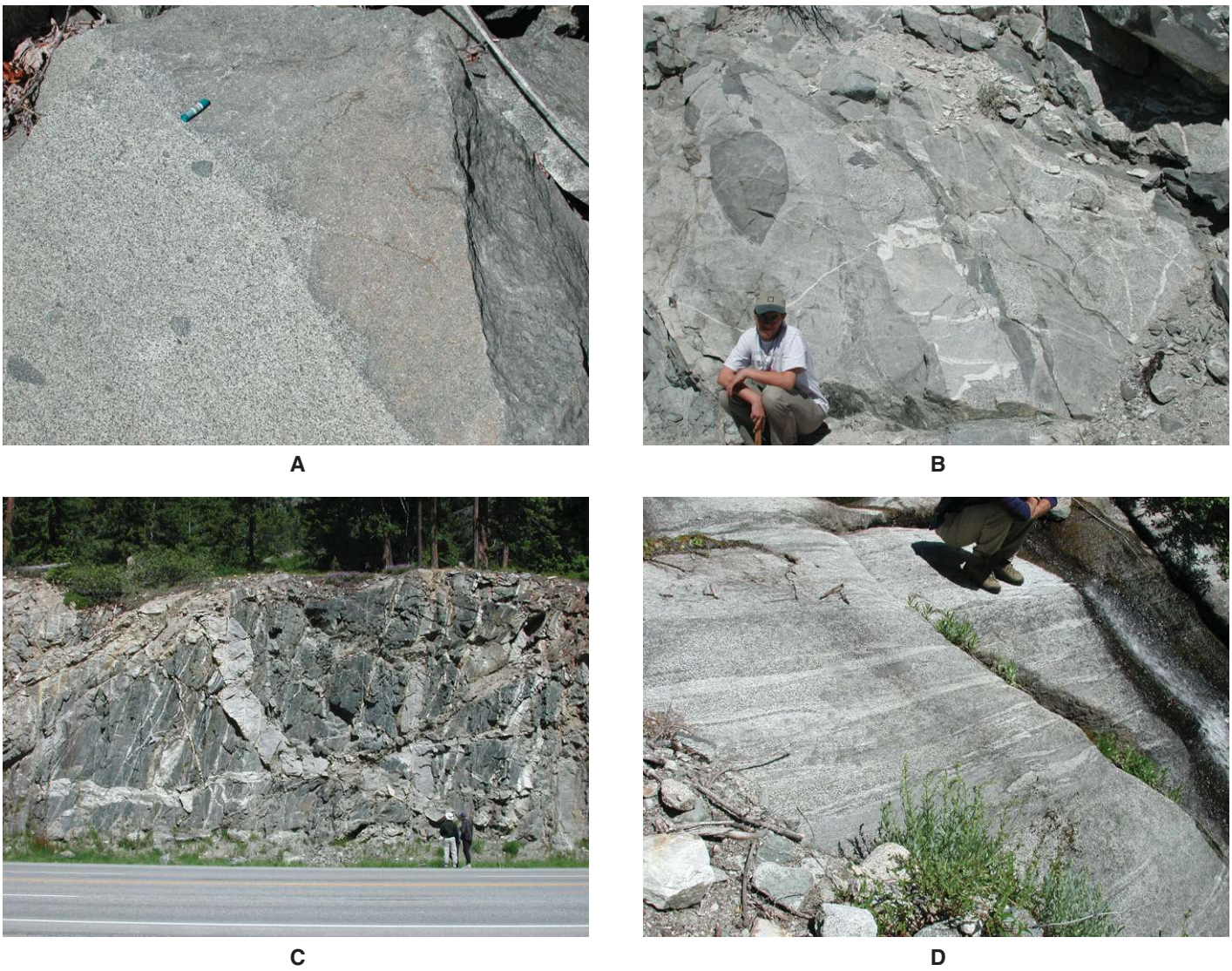

Figure 8. Outcrop photos from the Cascades core, Washington. (A) Simple sharp contact in the Mount Stuart batholith between the 94 Ma and 91 Ma pulse. Lip balm tube is ~6.5 cm long. (B) Crosscutting relationships of different pulses and mingling in the Entiat pluton. (C) Roadcut outcrop in the Nason Ridge Migmatitic Gneiss intruded by felsic dikes, an example of unfocused magmatism. (D) Sheeted complex in the Tenpeak pluton. Sheets are characterized by a variety of compositions and geochemistry signatures.

the normally zoned TB (Bateman and Chappell, 1979; Paterson and Vernon, 1995; Matzel et al., 2005; Žák and Paterson, 2005; Burgess and Miller, 2008; Miller et al., 2007; Economos et al., 2010; Memeti et al., 2010).

Implications for Magma Chamber Size and Pulses from the Magmatic Lobes

The Kuna Crest, Half Dome, and Cathedral Peak units all formed 10–60 km^2 magmatic lobes that intruded into the host rock and then were fairly isolated from the main batholith body. Although these smaller magma bodies have been mapped in the past as a single TB unit, the lobes are similar to the main TB in that they are characterized by normal zonation, i.e., exposing granodioritic to tonalitic units at the lobe margins and fine-grained leucogranites at their center and younging from margin to center (Memeti et al., 2010). Magmatic fabrics overprint gradational steep contacts between units. Element and isotope geochemistry suggest that the normal zonation is dominantly due to fractionation crystallization, with some prior mixing processes, and that the lobes may have been largely melt interconnected bodies early during their construction (Memeti et al., 2007, 2010).

Precise U-Pb zircon geochronology supported by thermal modeling (see following) indicates that magmatic lobes crystallized within 0.4–2 m.y. and thus had hypersolidus durations 20%–5% those of the main batholith (Memeti et al., 2010). These bodies potentially represent snapshots of simpler magmatic systems with less complex internal magma processes. They were mostly fed by a homogeneous source (i.e., the southern lobes, more complicated in the northern lobes) and did not interact with the main batholith body (Economos et al., 2010; Memeti et al., 2010). Our study suggests that the lobes are smaller bodies that were fed by either one pulse or several pulses that rapidly amalgamated to form 100–600 km^3 magma chambers (Memeti et al., 2010). The lobes intruded too far away from the locus of magmatism of the TB and

therefore failed to amalgamate with other pulses to form a larger, longer lived, magma chamber in which complex internal processes may have occurred over millions of years (Memeti et al., 2010). The full extent of the lobe magma chambers may have been reached fairly early during lobe construction due to magma pulsing that may have been fairly rapid (days to many thousand years?). In contrast, inward crystallization including fractionation, prolonged zircon crystallization (defined by the range of in situ crystallizing autocrystic zircons), and recycling likely took place over hundreds of thousands of years in a magma mush; nearly the entire longevity of the lobes (Memeti et al., 2010). Since neither the concentric normal zoning pattern nor the magmatic fabrics that overprint gradational contacts between lobe units were disturbed, we suggest that significant magma pulsing halted before the final compositional and structural patterns formed in the lobes.

Cascades Crystalline Core

Overview: Cascades Core

The crystalline core of the North Cascades (Cascades core) is the offset, southernmost extension of the >1500-km-long Coast belt of the Northwest Cordilleran orogen (Figs. 7 and 8), which underwent mid-Cretaceous crustal shortening and metamorphism during final suturing of the Insular superterrane to North America (Rubin et al., 1990; Journeay and Friedman, 1993). The Cascades core includes oceanic, island-arc, and clastic-dominated terranes that were mostly juxtaposed prior to the peak of mid-Cretaceous amphibolite facies metamorphism, arc-normal shortening, and magmatism (e.g., Brandon et al., 1988; Tabor et al., 1989). Regional shortening resulted in crustal thickening and burial of supracrustal rocks to depths of 25 to ≥40 km in many parts of the orogen (Whitney et al., 1999; Valley et al., 2003). Ductile structures in the southwestern part of the Cascades core predominantly formed in the mid-Cretaceous (e.g., Tabor et al., 1989; Paterson et al., 1994; Miller and Paterson, 2001b), whereas the northeastern part of the core recorded younger deformation coincident with ca. 78–45 Ma magmatism (Haugerud et al., 1991; Hurlow, 1992; Paterson et al., 2004; Miller et al., 2006).

In Miller et al. (2000, 2009) and Miller and Paterson (2001a), post-Cretaceous folding and faulting were qualitatively retrodeformed and a Cascades crustal column was established (Fig. 9C), constrained by thermobarometry (Brown and Walker, 1993; Evans and Davidson, 1999; Whitney et al., 1999; Valley et al., 2003). This column exposes both host rocks

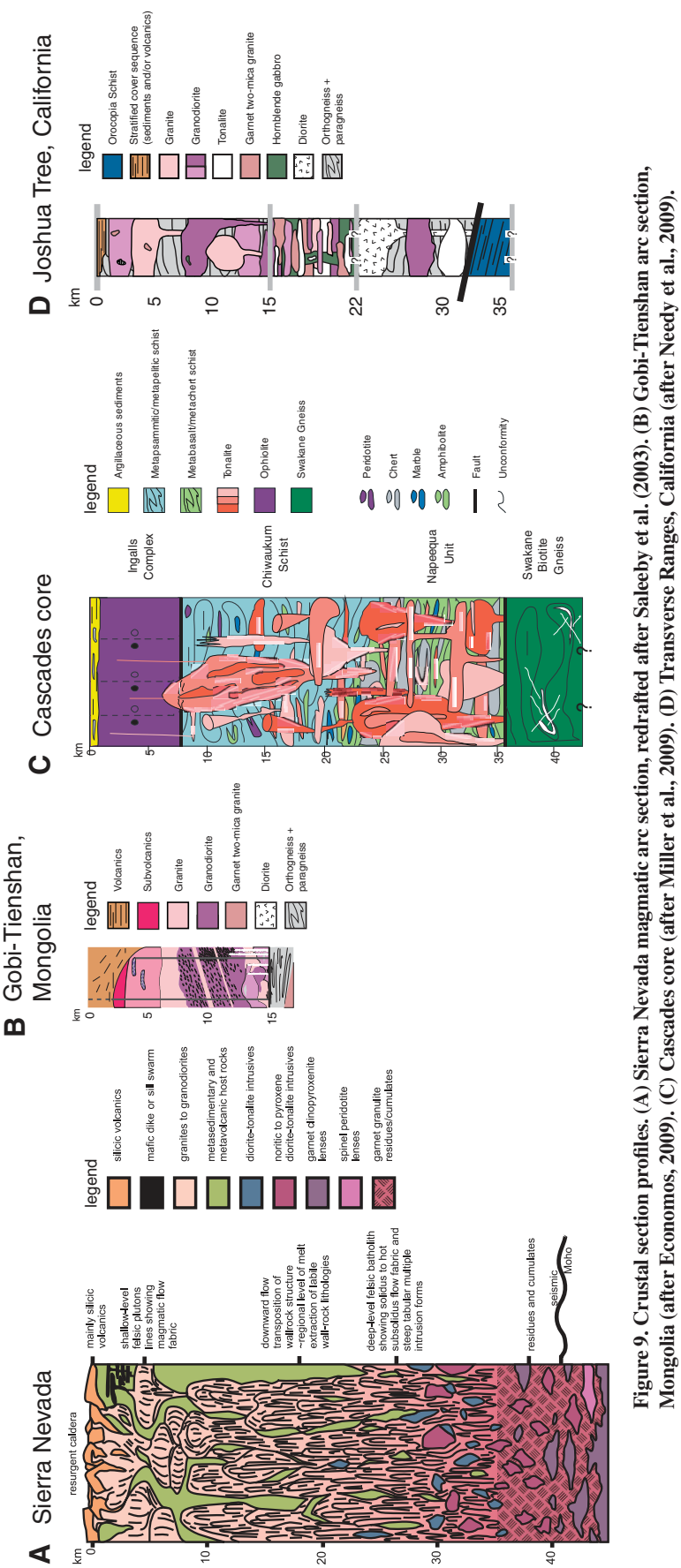

Figure 9. Crustal section profiles. (A) Sierra Nevada magmatic arc section, redrafted after Saleeby et al. (2003). (B) Gobi-Tienshan arc section, Mongolia (after Economos, 2009). (C) Cascades core (after Miller et al., 2009). (D) Transverse Ranges, California (after Needy et al., 2009).

and magmatic systems from ~5 to ~35 km depths. The nature of magmatic systems in this crustal column was discussed in detail in Miller et al. (2000, 2009), and therefore only a brief summary of those findings is presented herein.

The shallowest level of the crustal section is represented by the polygenetic Jurassic Ingalls ophiolite complex, which is dominated by ultramafic mantle tectonites (Miller, 1985; Miller and Mogk, 1987; MacDonald et al., 2008). The mid-Cretaceous Windy Pass thrust forms the lower boundary of the ophiolite (Miller, 1985). In the footwall of the thrust, the Chiwaukum Schist and related Tonga Formation and Nason Ridge Migmatitic Gneiss form the Nason terrane (Figs. 7 and 9C). The Chiwaukum Schist predominantly comprises pelitic and psammitic schist with Late Jurassic(?) and Early Cretaceous protoliths (Brown and Gehrels, 2007), and lesser amphibolite and ultramafic lenses (e.g., Plummer, 1980; Tabor et al., 1987; Paterson et al., 1994). The Chiwaukum Schist grades structurally downward into the Nason Ridge Migmatitic Gneiss, which consists of schist and paragneiss that resemble Chiwaukum rocks, but are extensively intruded by tonalitic sheets (e.g., Magloughlin, 1993; Tabor et al., 1987, 1993; Paterson et al., 1994). Metamorphic pressures are lowest at the southern end of the Chiwaukum Schist and increase from ~3 to 9 kbar at temperatures of ~540–700 °C over an ~10 km distance northeast from the Mount Stuart batholith. The Nason terrane is likely underlain by the Napeequa complex (Napeequa Schist of Cater and Crowder, 1967; Miller and Paterson, 2001a; Brown and Dragovich, 2003; Miller et al., 2009). The Napeequa complex consists mainly of amphibolite, quartzite, and biotite schist; minor metaperidotite and marble are also present. These rocks were metamorphosed to ~8–11 kbar (Brown and Walker, 1993; Valley et al., 2003). The base of the Napeequa complex is the Dinkelman décollement, which places the unit over the metapsammitic Late Cretaceous Swakane Gneiss (Figs. 7 and 9C; Paterson et al., 2004). The Swakane Gneiss was underthrust beneath the Napeequa unit between ca. 72 and 68 Ma to depths corresponding to pressures reaching 12 kbar (Valley et al., 2003; Matzel et al., 2004).

Cascades Core Magmatism

Cretaceous magmatic bodies are distributed throughout the crustal section (Fig. 9C). Plutons are dominantly tonalite (Misch, 1966; Cater, 1982; Dawes, 1993). Diorite and gabbro are subordinate components of most intrusions; granodiorite is found in variable amounts (Misch, 1966). Dawes (1993) and DeBari (DeBari et al., 1998; Miller et al., 2000) inferred from geochemical data that the dominant tonalites formed by variable mixing of mantle-derived mafic magmas with lower crustal melts (felsic tonalite, trondhjemite, granodiorite). The ε_{Nd} values of +6.3 to +1.5 also likely record mixing of mantle-derived melt with melt formed by partial melting of isotopically juvenile terranes (Matzel et al., 2008). Rare earth element patterns indicate a garnet-bearing mafic source for the crustal melts (Miller et al., 2000), and pressures of ~15–16 kbar are inferred for melting (De Bari et al., 1998; Miller et al., 2000).

Incremental Growth and Shapes of Plutons

Pluton shapes in the Cascades core can be generalized into four broad categories: (1) asymmetric wedges to funnels that are elliptical in map view; (2) subhorizontal tabular bodies; (3) steep-sided, blade-shaped bodies with high aspect ratios in map view; and (4) steep-sided, vertically extensive (~10 km or greater) bodies that are complexly shaped to elliptical in map view (Figs. 7, 8, and 9C; Miller et al., 2009). Many have minimum vertical extents of 5 km, and have high aspect ratios in map view. Thin (<5 km) subhorizontal tabular bodies are more common with depth and are best represented at depths of >20 km; however, steep sheeted (blade-shaped) bodies and wedge-shaped plutons are also present at these levels. Thus there is considerable diversity in the geometry of Cascades plutons.

Magmatic sheeting, and thus potential evidence of incremental growth, occurs at all crustal levels, but is increasingly widespread at greater depths. Sheeting occurs in several settings: (1) along the margins of large elliptical to steeply dipping, sheet-shaped plutons (e.g., Tenpeak and Entiat plutons; Figs. 7, 8B, 8D, and 9C); (2) throughout some mid- to deep-crustal sheeted plutons (e.g., Cardinal Peak and Dirtyface plutons); and (3) in fairly complicated dike and/or sill complexes in which individual sheets have highly variable orientations and are often separated by sections of host rock (Fig. 8C). The first two result in focused magmatic systems, whereas the latter indicates a fairly unfocused system. In the following we briefly describe three well-dated Cretaceous plutons, which were emplaced at widely different levels, and illustrate a variety of styles of pluton growth.

Mount Stuart Batholith

There is also both field and geochronologic evidence that the large focused magmatic systems also grew incrementally. For example, at moderate, ~2–4 kbar crustal levels, the 96.3–90.8 Ma Mount Stuart batholith consists of a larger (~480 km^2) northeast body and a smaller southwest body; the northeast body has a southeastern mushroom-shaped region, the stem of which extends into a central sheet-like segment, and a northwestern hook-shaped region (Figs. 7 and 8A). The hook-shaped region consists of granodiorite, which grades to the southeast into tonalite that also makes up the central sheet-like segment. In the mushroom-shaped region, tonalite dominates, grades into granodiorite in the center, and surrounds two-pyroxene gabbro and diorite to the east (Erikson, 1977; Tabor et al., 1987; Paterson et al., 1994). Matzel et al. (2006a) divided the batholith into four age groups. The oldest rocks are 96.3–95.4 Ma and are in the hook region and a gabbro outlier. The next age group is represented by the tonalite in the sheet-like region, followed by tonalite in the "stem" of the mushroom-shaped region (Matzel et al., 2006a). The youngest (90.9–90.8 Ma) and most voluminous age domain consists of gabbro, tonalite, and granodiorite in the mushroom-shaped region (Figs. 7 and 8A). Matzel et al. (2006a) concluded from these age data that the batholith was constructed by short periods of high-magma flux (volume addition rates using our terminology) separated by magmatic lulls; they also demonstrated that a minimum of 500 km^3 of magma was intruded over an interval of ~200 k.y. (ca. 91 Ma) and that a large magma reservoir existed at that time.

Seven Fingered Jack and Entiat Plutons

A 20-km-wide zone in the Chelan block contains ca. 92–71 Ma plutons, which consist of steep, centimeter- to kilometer-scale sheets emplaced at ~20–25 km depths (e.g., Hurlow, 1992; Dawes, 1993; Paterson and Miller, 1998; Miller and Paterson, 2001a; Matzel, 2004). The 92–90 Ma Seven Fingered Jack pluton and a 79 Ma gabbro sheet in the northwest are contiguous with the 73–71 Ma Entiat pluton in the southeast and form a <10-km-wide, dominantly tonalitic plutonic complex that extends for >80 km (Figs. 7 and 8B). Sheets of heterogeneous mafic rocks (hornblende gabbro and diorite) and hornblendites are mingled with tonalites and trondhjemites in the margins and northwest tips of overlapping sheets of the Seven Fingered Jack intrusion. Inward from these thinly sheeted zones are thicker sheets of medium-grained hornblende-biotite tonalite and an interior sheeted body of biotite granodiorite. The Entiat pluton is more homogeneous than the older Seven Fingered Jack unit. Mafic sheets are abundant in the southwest margin and a 3.5-km-wide body of two-pyroxene gabbro and diorite makes up part of the northeast margin of the intrusion. These mafic units grade inward into the thicker (>50 m) sheets and less elongate masses of coarse-grained hornblende-biotite

tonalite, which have more cryptic internal contacts. Rafts and xenoliths of host rocks are abundant between and within marginal sheets of both plutons. U-Pb data of Matzel (2004) from the plutons indicate that numerous sheets contain concordant zircons dispersed over a 2–3 m.y. time span. Matzel (2004) interpreted the zircon inheritance patterns to record partial disaggregation and mixing of slightly older, partially solidified sheets into the younger sheet near the level of emplacement. During this process, older zircons were incorporated into the younger sheet. In summary, the age data and field relations support a history of incremental assembly by sheeting over intervals of 2–3 m.y. for construction of two sizeable (≥200 km^2 each) plutons.

Tenpeak Pluton

The best-studied deep focused intrusion in the Cascades core is the 92.3–89.7 Ma Tenpeak pluton (Figs. 7 and 8D; e.g., Cater, 1982; Dawes, 1993; Miller and Paterson, 1999; Matzel et al., 2006a). This 7–9 kbar (emplacement depth) pluton is broadly elliptical in map view with a <500-m-wide, discontinuous heterogeneous zone of mingled and sheeted gabbro, tonalite, and hornblendite along its margin (Cater, 1982; Miller et al., 2000). Inward from this mafic zone is voluminous tonalite and in the north, diorite and mafic garnet-bearing tonalite. Within the tonalite, a ca. 92.2 Ma phase overlaps in age with the mafic zone. Less than 0.3 m.y. later, sheets were injected in an internal zone that contains numerous meter-scale inclusions of amphibolite and metaperidotite (Matzel et al., 2006a). Tonalitic magmatism continued at 91.3 Ma in the northeast margin and at 90.6 Ma in the north end (Fig. 7), and was followed by an apparent hiatus before intrusion at 89.7 Ma of distinctive coarser grained tonalite that truncated the sheeted zones (Miller and Paterson, 1999; Matzel et al., 2006a). Matzel et al. (2006a) concluded that magma volume addition was broadly distributed during the 2.6 m.y. of pluton construction. Thus the detailed high-precision geochronological data from the Mount Stuart batholith and Tenpeak pluton indicate that both large blob-like plutons and more elongate, partly sheet-like bodies grew over relatively long time periods (2.7–5.6 m.y.; Matzel et al., 2006a).

Cascade Core Magma Plumbing System

Plutons are often considered as isolated entities; however, we note that many of the Cascade plutons are probably thicker, trapped parts of fairly continuous magma plumbing systems. We envision that many of the plutons pass upward and downward into both thicker and thinner magmatic bodies, and complex lateral changes may also be present (Fig. 9C). In Miller et al. (2009), these relationships were interpreted in terms of the following model for 96–72 Ma Cascades magmatism. Magmas encompassing variable proportions of mantle and crustal melts rose to a wide range of crustal levels. These magmas ascended in broadly arc-parallel, magma transfer zones during regional shortening. The elongate, vertically sheeted, deep- to mid-crustal bodies oriented at high angles to the regional shortening direction do not fit classic brittle diking mechanisms. We contend that it is more likely that magmas ascended through a network of channels (e.g., Weinberg, 1999; Brown, 2004) and/or as multiple pulses of narrow, elongate viscoelastic diapirs (Paterson and Miller, 1998; Miller and Paterson, 1999, 2001a). Early mafic sheets crystallized along the walls of the plutonic system. These earlier sheets were intruded by wider tonalite sheets, and a larger magma chamber eventually formed in the interior of the system. The amount of crustal melt presumably increased with time, probably as a result of progressive heating by underplating of mafic magmas. The vertically sheeted, partially molten bodies aided the ascent of subsequent magmas to higher crustal levels (e.g., Mount Stuart), where larger volumes of magma became more thoroughly hybridized, which led to internal gradational contacts. The final product is a complex three-dimensional system of variably connected plutonic bodies with a wide range of shapes and sizes.

Percentages of Plutonic and Host Rocks with Depth

Accumulation of Cretaceous magmas at shallow, middle, and deep levels in the Cascades core was quantitatively estimated in Paterson et al. (2004) and Miller et al. (2009). Areas of discrete plutons are easily calculated, but the amount of intrusive rock represented by the thin isolated sheets in the column is much less confidently determined. Our best estimates of the percentage of the latter types of intrusive rocks from areas we have studied in detail are extrapolated throughout the panel of rock under consideration, and are probably accurate to within 10%.

This analysis indicates that plutonic rocks are volumetrically significant at all crustal levels. The percentage of intrusive rocks increases systematically from shallow (37%), to middle (55%), to deep (65%) crustal levels (Fig. 9C; see Miller et al., 2009, Table 2 therein). Tonalite dominates at all crustal levels. Focused magmatism defined by discrete plutons and unfocused (dispersed) magmatism represented by typically <50-m-thick sheet-like and irregularly shaped bodies intruding metamorphic host rocks are present at all crustal levels, but are unevenly distributed. Unfocused magmas compose ~18% of the total plutonic rock in the deep crust and 19% at mid-crustal depths, but <1% at shallower levels. The two largest intrusions, the Mount Stuart and Black Peak batholiths, which were sites of intermittent magma accumulation for as long as 5.5 m.y., were emplaced at relatively shallow depths.

THERMAL MODELING

Introduction

The pioneering work of Jaeger and coworkers (e.g., Jaeger, 1961; Carslaw and Jaeger, 1959) paved the way for modern thermal studies of magmatic systems. Examples of subsequent studies include mid-ocean ridge magmatism (Sleep, 1975, 1991; Wilson et al., 1988), melt generation in the upper mantle and/or lower crust and above subduction zones (Liu and Furlong, 1992; Parsons et al., 1992; Peacock et al., 1994; Koyaguchi and Kaneko, 1999), arc magmatism (Hanson et al., 1993; Hanson and Barton, 1989), and volcanic systems (Carrigan, 1983; Furlong and Shive, 1983; Guillou-Frottier et al., 2000). Arc magmatism studies include the thermal viability of different emplacement models such as diapirism (Marsh, 1982), diking (Petford et al., 1994), extensional fault models (Hanson and Glazner, 1995; Yoshinobu et al., 1998), and stoping (Marsh, 1982; Furlong and Myers, 1985). Models of internal chamber processes include fractional crystallization and solidification fronts (Marsh, 1996; Kuritani, 1999), magma mixing (Sparks and Marshall, 1986; Blake and Fink, 2000), assimilation (Clarke et al., 1998; McLeod and Sparks, 1998; Pignotta et al., 2001a, 2001b), and extraction for volcanic eruptions (Carrigan, 1983; Furlong and Shive, 1983; Guillou-Frottier et al., 2000).

Only a few studies specifically examined the thermal evolution of incrementally constructed magma chambers (Sleep, 1975; Hanson and Glazner, 1995; Yoshinobu et al., 1998; Annen et al., 2006a, 2006b; Paterson et al., 2007). Comparing volume addition rates and volumetric fluxes between 1-D, 2-D, and 3-D thermal models and to 2-D or 3-D estimates in natural systems is problematic because assumptions about the systems in the missing dimensions, in what part of the systems volumetric fluxes are calculated, whether instantaneous or long-term volumetric fluxes are considered, and means of normalizing calculations to identical areas are all challenging (discussed herein). However, these studies of incrementally grown systems clearly show the first-order importance of volumetric fluxes and their spatial distributions in controlling the thermal history of magma chambers, and also exemplify additional critical factors

such as initial host and magma temperatures and shapes of magma pulses. The above-cited studies focused on sheet-shaped pulses and relatively small volume systems. Our studies of large intrusions in a number of arcs have motivated us to compare the above studies to the thermal evolution of volumetrically large bodies formed by a few too many pulses (Figs. 10–14). Here we present a full range of scenarios (different pulse shapes and sizes and fluxes) with the goal of evaluating the sizes and durations of magma chambers in both small- and large-volume systems.

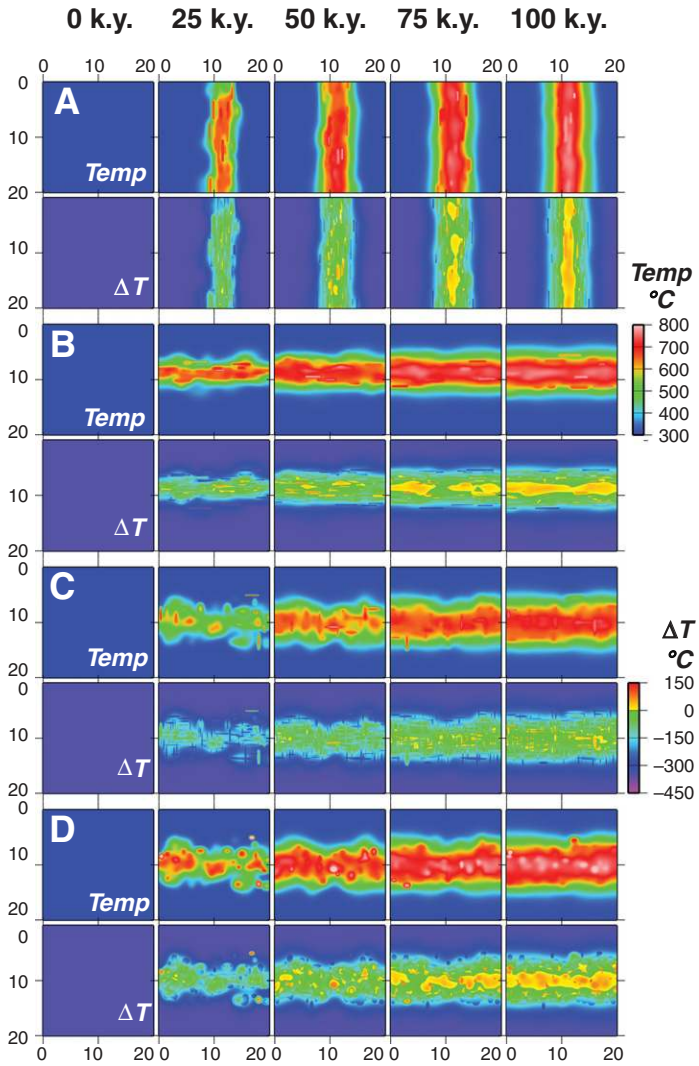

Figure 10. Thermal modeling results of dike and/or sheet complexes of rectangular or elliptical geometry emplaced at any time, shown in 25 k.y. time panels (modeling parameters in Appendix Table A2). For each model, temperature evolution (Temp) and temperature relative to solidus temperature (ΔT) are shown. (A) Vertical dikes. (B) Sills. (C) Vertical and horizontal dikes. (D) Blob-like shapes. (Magma addition rates and volumetric fluxes for these two-dimensional models are listed in Appendix Table A3.)

Thermal Code

Our modeling strategy uses finite difference implementation of 2-D heat conduction equations in a manner that allows us to create the thermal evolution of incrementally growing intrusions constructed through the amalgamation of pulses with variable properties. Finite difference methods offer full spatial heterogeneity of rock types and properties, fine-scale internal grid spacing that allows for the definition of intricate rock geometries, and small internal time steps for calculations over any time duration (Croft and Lilley, 1977; Furlong and Myers, 1985; Bejan, 1995). Careful code construction for numerical stability, computational efficiency, and resource management (dynamic memory allocations and central processing unit parallelization) allows us to model at scales between submeter to kilometers for time durations of days to millions of years. Several types of initial and boundary conditions are installed, including constant, absorbing, thermal gradients, and heat flux (mW/m^2). Geothermal gradients can be defined by linear gradient boundaries or by assigning radiogenic heat production to mesh nodes. The effects of latent heat of fusion can be included or switched off in the thermal modeling. This effect is implemented at each node by absorbing or releasing heat based on latent heat of fusion release temperatures and properties. The 2-D mesh in the code is deformable by expansion that emulates extension or can mimic multiple pulses by overprinting appropriate nodes with different rock properties.

We have modeled a number of geological scenarios (Appendix Table A2): (1) Single intrusions of rectangular or elliptical geometry can be emplaced at any time; these shapes can have any orientation, aspect ratio, and position (i.e., sills, dikes, or blobs; Fig. 10). (2) A sequence of intrusions can be emplaced at specified but arbitrary times or according to a time rate (Figs. 10–14). Shapes in the sequence can be fixed (Figs. 11 and 12) or be set to randomly vary (via linear or Gaussian distributions) within a range of dimensions, aspect ratios, and positions (Fig. 10), resulting in laterally variable volumetric fluxes (Appendix Table A2). (3) A sheeted dike complex can be created wherein the thermal model actually expands according to a growth (extension) rate to accommodate the emplacement of new, but thin dikes (Fig. 11). Dike width and the time between dikes are coupled based on growth rate; our code allows each of these to be varied. (4) Irregular shapes from maps or cross sections can be entered into the thermal codes by rendering digital scans into modeling domains, which are then assigned rock types and associated thermal properties (Figs. 13 and 14). These mapped shapes are emplaced into the thermal model at specified times so that they represent new thermal pulses, which alter the conducting thermal field. The use of maps or cross sections allows us to examine the thermal behavior of actual observed field geometries. Using these geological scenarios, we examine the fine-scale thermal effects of episodic intrusion using pulses of a large range of sizes, shapes, positions, and recurrence intervals. To analyze reservoir construction and duration, we calculate ΔT, the per-node difference between the modeled temperature field

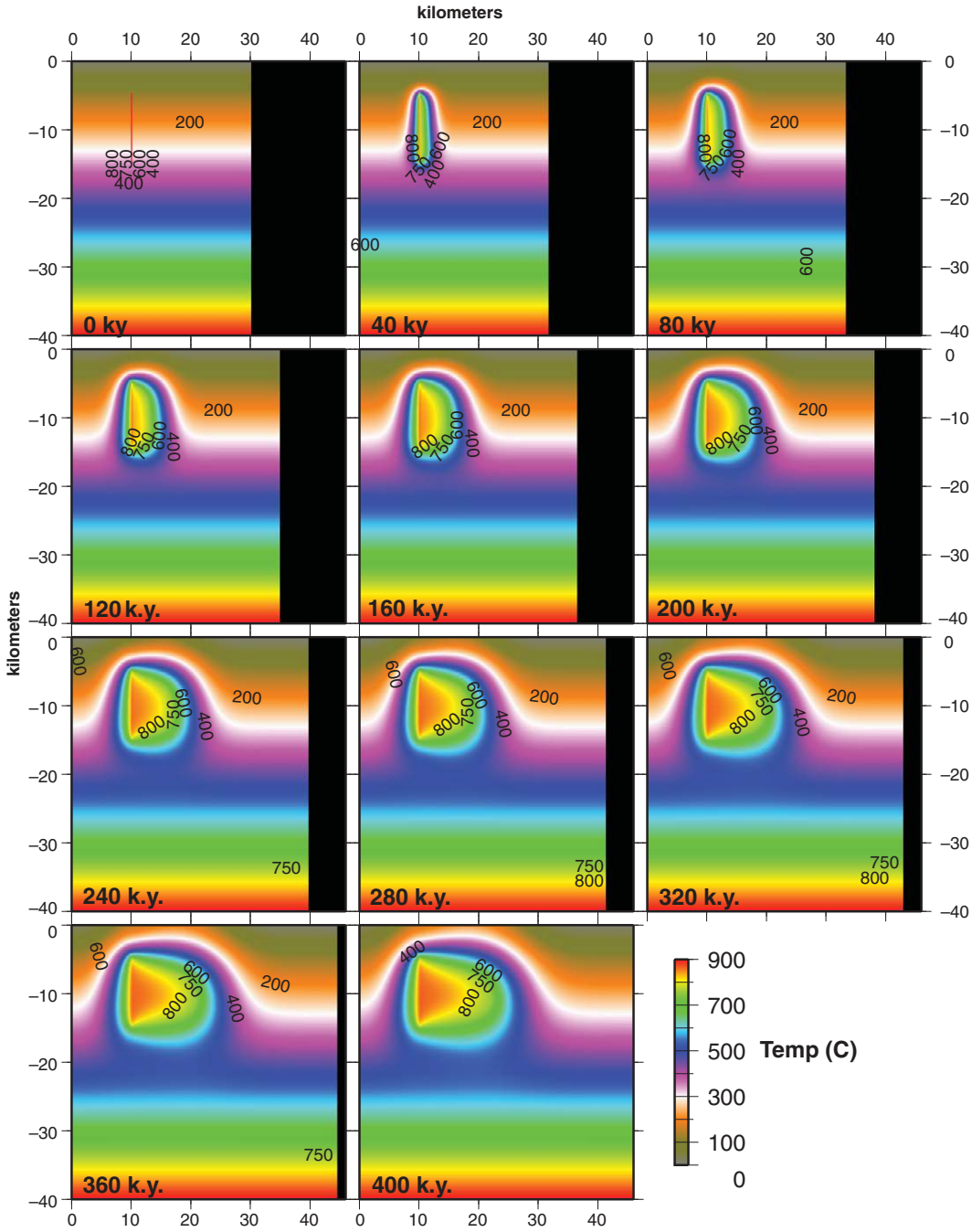

Figure 11. Thermal modeling results of a sheeted dike complex wherein the thermal model expands according to a growth (extension) rate to accommodate the emplacement of new but thin dikes. Dike width and the time between dikes are coupled based on growth rate; our code allows each of these to be varied. Time panels of 40 k.y. are shown. Modeling parameters are in Appendix Table A2. Magma addition rates and volumetric fluxes are shown in Appendix Table A3.

and the rock solidus temperature where positive values represent hypersolidus conditions and the presence of melts.

Thermal Modeling Results

Sheeted (Dike, Sill, Lopolith, Small Blobs) Complexes

We have examined a group of scenarios in which a large number of small magma pulses, with variable sizes, shapes, orientations, and locations, are emplaced within a restricted region of the crust. These scenarios result in vertically oriented sheeted dike complexes (Fig. 10A), horizontally oriented sill complexes (Fig. 10B), clustered by otherwise random dike and/or blob complexes (Figs. 10C, 10D), and vertically oriented sheeted dike complexes controlled by fault motions (Fig. 11; see also Yoshinobu et al., 1998; Annen et al., 2006b). Attempting to construct any of these scenarios exemplifies the challenges of developing robust thermal models. One must decide on (1) the size, shape (aspect ratio), and orientation of the sheets; (2) how often new sheets are emplaced (long-term volumetric flux, recurrence interval, and size of sheets are obviously closely linked); (3) the location and/or randomness of sheet emplacement; (4) the initial magma and host temperatures; and (5) what happens to previous host rock (including earlier magma pulses) when a new sheet is emplaced. Each of these is controlled in our code (Appendix Table A2) and each will affect the resulting thermal history. Thermal histories during the initial emplacement of sheets are highly variable

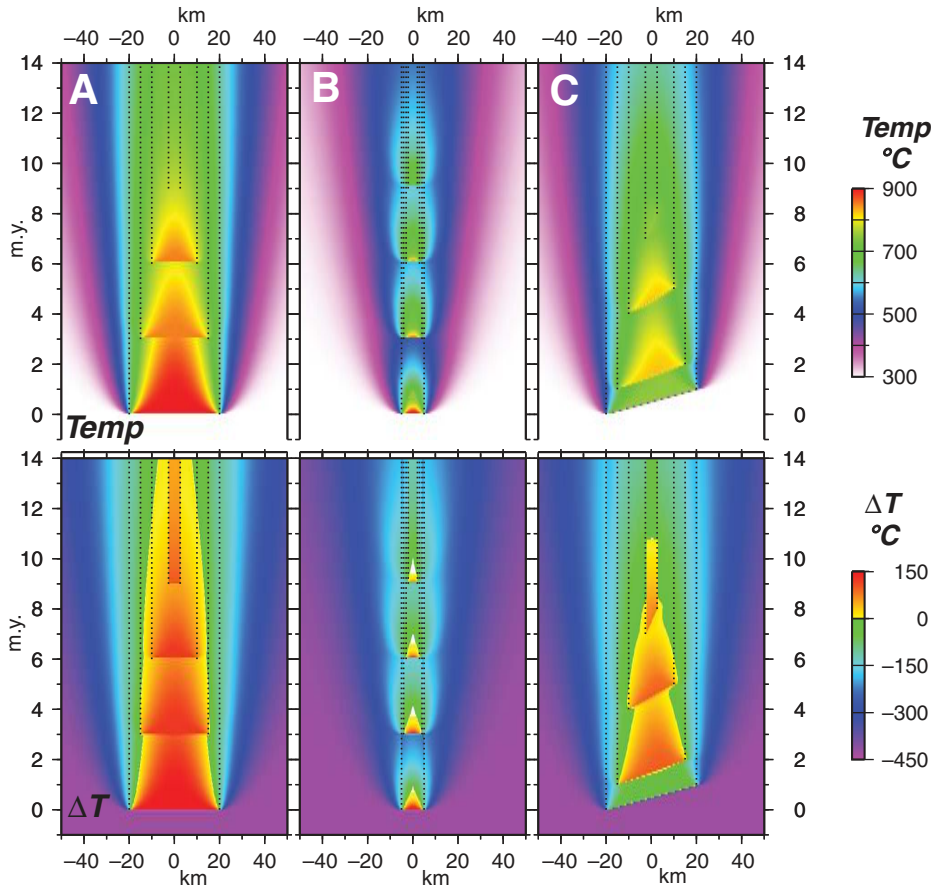

Figure 12. Thermal modeling results of nested cylindrical pulses using Tuolumne batholith time scales of intrusion. (A) Starting pulse width = 40 km. (B) Starting pulse width = 10 km. (C) Pulses constructed by incremental growth. First pulse is growing from left to right for 40 km for 1 m.y. Temperature (Temp) and temperature relative to solidus temperature (ΔT) are shown. Modeling parameters are in Appendix Table A2. Magma addition rates and volumetric fluxes are shown in Appendix Table A3.

(rapid increase and decrease in temperatures in the middle and upper crust).

Calculations of total added volumes, volume addition rates, and volumetric fluxes for the sheeted complexes are summarized in Appendix Table A3. In Figure 10 the volume addition rates range between 2.27×10^3 and 3.64×10^3 km^3/m.y. and the volumetric fluxes range between 1.14×10^2 and 3.46×10^2 km^3/km^2/m.y. The magma reservoir built by thin dikes emplaced at a stationary feeder location (Fig. 11) grows at a rate of 4.0×10^2 km^3/m.y. The associated volumetric flux is 2.5×10^1 km^3/km^2/m.y. if measured over the final reservoir width, but is 4.0×10^3 km^3/km^2/m.y. if measured based on the width of the feeder dike (Appendix Table A3). In all cases, if the long-term magma volumetric flux is moderate to high and/or magma pulses are spatially focused, the overall temperature rises fairly rapidly above the magma solidus, typically within 75 k.y. in the scenarios used to construct Figures 10 and 11, and magma chambers grow that will have sizes and durations much greater than the sizes and hypersolidus histories in individual sheets. For example, Yoshinobu et al. (1998) showed that magma chambers grown by dike-shaped pulses in fault-controlled settings typically formed in <50 k.y. in many geologically realistic scenarios (volume addition rate of 4.0×10^2 km^3/m.y. and fluxes of 2.5×10^1 km^3/km^2/m.y.), particularly with increasing crustal depths (Fig. 11). As volumetric fluxes increase, it is common for magma chambers to form that are much larger than individual pulses and last well over 500 k.y. (Figs. 10 and 11).

Nested Vertical Cylinders (Nested Diapirs or Incrementally Grown Diapir-Like Pulses)

Another end-member model, traditionally suggested for large, normally zoned plutons, is that a few, larger batches of magma, rising as diapirs, are nested within one another, since younger pulses, utilizing the same magma pathway, tend to move up the hotter and weaker centers of the older pulses (Stephens, 1992; Paterson and Vernon, 1995). Debate continues about whether the host rock and earlier magma batches were displaced sideways (ballooning models) or vertically to allow ascent of the younger pulses (e.g., Paterson and Vernon, 1995; Clemens, 1998). Our field studies of a number of these plutons resulted in observations indicating that older material is moving either up or down rather than sideways (e.g., Paterson and Vernon, 1995; Paterson and Farris, 2008). It is also likely that some of these large pulses were incrementally constructed either by earlier amalgamation of smaller pulses, continuous arrival of magma into a chamber, or continued rise of a tail of a diapir. We can begin to thermally explore these models by considering nested cylinders during which instantaneous arrival of a new pulse is represented by superposition of new rock properties and temperatures without any lateral translation in the model. We have examined scenarios starting with 40- and 10-km-diameter vertical cylinders with each subsequent cylinder having smaller diameters (Figs. 12A, 12B), resulting in long-term volume addition rates of 2.52×10^8 to 1.86×10^7 km^3/m.y. and fluxes of 2.75×10^4 km^3/km^2/m.y. (these fluxes occurring over many adjacent kilometers). In the former case (Fig. 12A), magma chambers remain above their solidus for many millions of years if new pulses are brought in every 2–3 m.y. or less. This scenario is not geologically realistic over long time scales because it requires large volume addition rates of magmatism and is not supported by known cooling histories of plutonic bodies. For the 10-km-diameter scenario, magma chambers survive for ~1.0 m.y. if recurrence interval between pulses is greater than a few million years (Fig. 12B). If the time between pulse arrivals is shorter, then longer lived chambers will occur. This draws attention to the crucial control of the long-term volumetric flux, recurrence interval between pulses, and spatial distribution of the fluxes.

We also examined this scenario (with the same long-term volume addition rate), but with each large pulse or cylinder constructed by many smaller dike-shaped increments over a million years duration (volumetric flux of 2.5 km^3/km^2/m.y.; Fig. 12C). If these increments arrive over a shorter duration relative to the interval between arrivals of the large pulses (1:3 m.y. in Fig. 12C), then although the initial thermal history is more variable, the long-term fluxes, thermal history, and the resulting sizes and durations of magma chambers are quite similar to the above results.

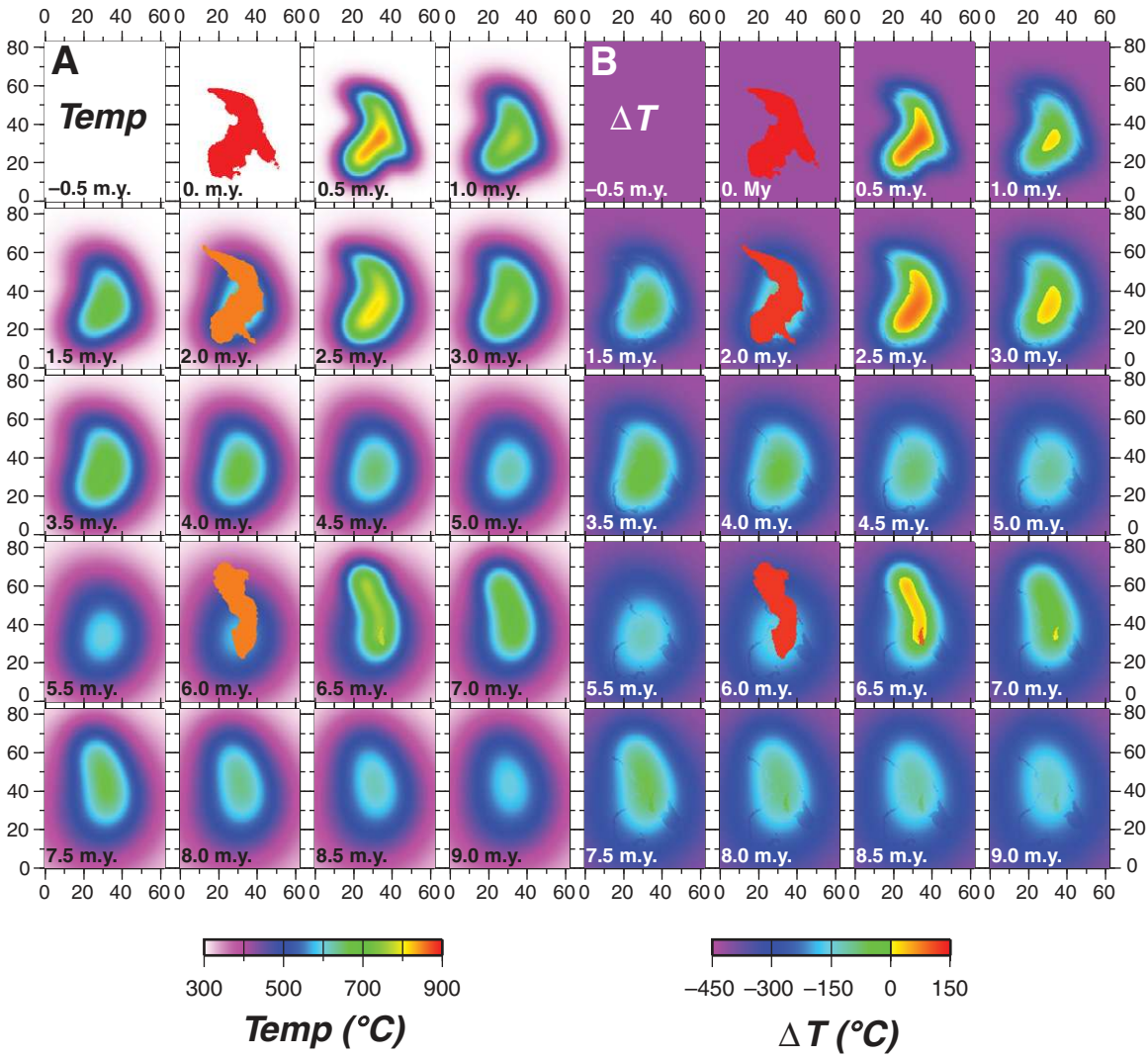

Figure 13. Thermal modeling results using irregular shapes from maps, here the Tuolumne batholith example. Mapped shapes are emplaced into the thermal model at specific times known through U-Pb zircon geochronology (see also Fig. 5) so that they represent new thermal pulses, which alter the conducting thermal field. (A) Thermal model results showing temperature (Temp) evolution. (B) Thermal model results showing temperature relative to solidus temperature, ΔT. Modeling parameters are in Appendix Table A2. Magma addition rates and volumetric fluxes are shown in Appendix Table A3.

Irregular Mapped Shapes

Another approach we are exploring is to scan actual mapped shapes of plutonic bodies, rasterize and enter them into the thermal codes, and then assign rock types and thermal properties (Fig. 13). Decisions must be made about their thickness in the third dimension, which mapped portions represent different pulses, to what degree older pulses were affected by younger pulses (e.g., were parts of older pulses removed?), and the timing of pulse arrival (based on relative timing and geochronology) in the thermal model. We use the TB as a case study (Figs. 5 and 13). We use new 1:24,000 mapping of much of the batholith (Žák and Paterson, 2005; Memeti et al., 2010) and new high-precision U-Pb zircon geochronology (Mundil et al., 2004; Matzel et al., 2005, 2006b; Memeti et al., 2010) to examine thermal histories of different emplacement scenarios (e.g., 4 large diapiric pulses and/or numerous dike-shaped pulses resulting in long-term fluxes of 4.0×10^4 km^3/km^2/m.y. at three scales): (1) small irregularities along the batholith margin, (2) moderate-sized lobes extending away from the main chamber, and (3) the even larger central batholith (Fig. 13). In most likely scenarios, the irregular margins and marginal portions of lobes solidify rapidly in <<50 k.y.; lobe centers maintain magma chambers as long as 500 k.y., or even longer where lobes merge with the main chamber. In the main batholith, magma chambers have durations of ~1 m.y., locally increasing to ≥2 m.y. depending on the recurrence interval and emplacement location of younger pulses. Another intriguing conclusion is that younger pulses tend to be centered (first arrive?) in the regions of highest existing temperature isotherms, suggesting a likely rheological control on magma ascent in these nested systems.

Nested Disks with Irregular Mapped Shapes

We have used the above-described irregular mapped shapes and added variable thicknesses to them, resulting in irregular hockey

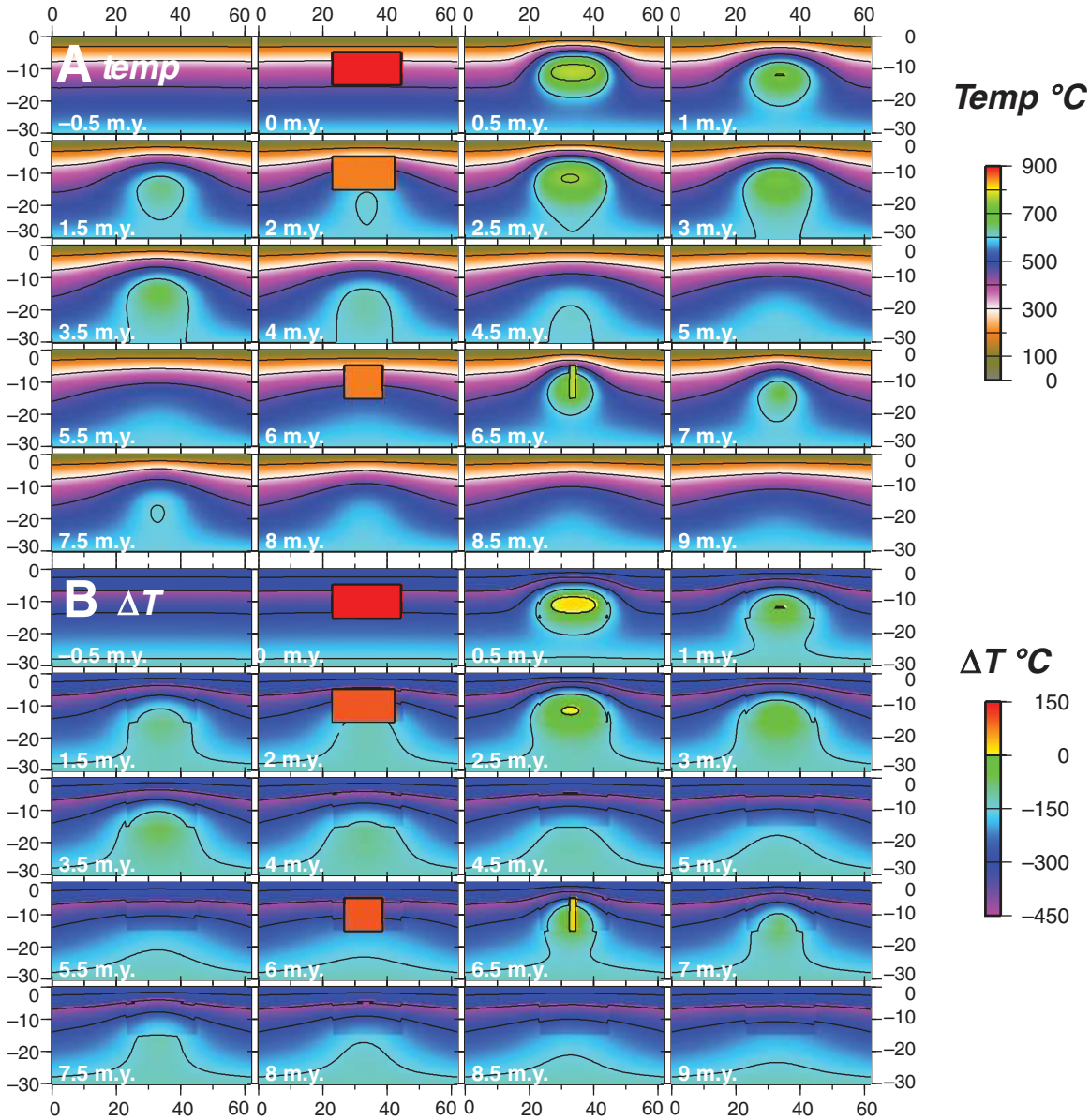

Figure 14. Thermal modeling results showing vertical sections through irregular, nested hockey puck–shaped bodies, here the Tuolumne batholith example. Pluton thickness estimated through mapped shapes. Hockey puck–shaped bodies are emplaced into the thermal model at specific times, similar to Figure 13. (A) Thermal model results showing temperature (Temp) evolution. (B) Thermal model results showing temperature relative to solidus temperature, ΔT. Modeling parameters are in Appendix Table A2. Magma addition rates and volumetric fluxes are shown in Appendix Table A3.

puck–shaped bodies, and then emplaced these in crust with variable geothermal gradients (Fig. 14). Using the TB as a case study with similar fluxes to those described above, and in spite of the variables introduced in these models, the size and durations of magma chambers are comparable to those noted above in the discussion of Irregular Mapped Shapes; the most important controls are the magma volumetric flux, vertical thickness of pulses, and the crustal depth of the system. It is common in these scenarios to have magma chambers in the upper crust that naturally decrease in time but still have durations of >1 m.y.

Processes that Increase or Decrease Cooling Times

A number of processes can significantly increase or decrease the cooling and solidification times of magmatic bodies (Furlong et al., 1991). Effects that will speed up cooling include (1) possibly 3-D cooling, particularly in certain scenarios such as magma emplacement at shallow depths and in thin subhorizontal sheets, although recent studies indicate that this 3-D cooling effect, particularly for larger bodies, may not be as significant as previously thought (e.g., Jaeger, 1961; B. Marsh, 2010, personal commun.); (2) advective cooling through internal convection, transport of magma from chambers into colder host rocks, transport of cold rock into the magma chamber, or development of a

hydrothermal system around the body; (3) starting with colder magma or host-rock temperatures, or lower geothermal gradients; (4) lower long-term volumetric fluxes; (5) greater spatial distribution of magma bodies; and (6) thinner magma bodies.

Effects that will increase crystallization and cooling times are (1) hotter starting magma or host-rock temperatures; (2) higher geothermal gradients and/or deeper crustal levels; (3) higher long-term volumetric fluxes; (4) additional magma pulses passing through the system, as would occur when a batch moves up through a magma plumbing system and/or during a volcanic eruption; (5) thicker bodies and/or bodies with lower aspect ratios; (6) spatial nesting or focusing of magma pulses; and (7) lower thermal conductivity of melt, as determined by Whittington et al. (2009).

Most of these effects are issues specific to natural systems and may vary dramatically from system to system. Some of these effects are already under examination; for example, we are testing to see to what extent hydrothermal systems cooled the TB, and initial results indicate that this is not an important process during the crystallization of this batholith (Lackey et al., 2008; Paterson et al., 2009; Clemens-Knott, 2009, personal commun.).

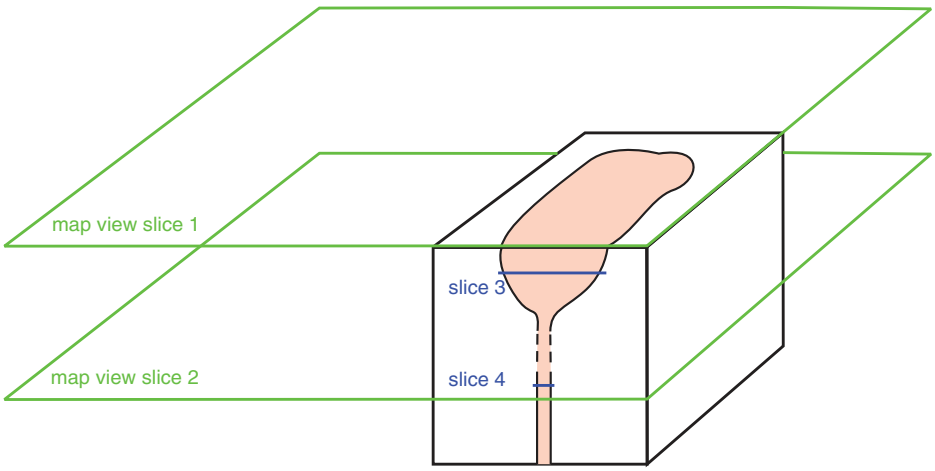

Figure 15. Simple magmatic system (see Figs. 5, 7, and 9 for more realistic systems) showing different scales and locations over which magmatic addition rates and volumetric fluxes are typically calculated. Map slices 1 and 2 potentially represent regional areas (100 km^2 or ~1° arc length) over which average long-term rates are determined, but represent two different crustal levels that may give two different results if based on preserved plutonic material. Slices 3 and 4 represent localized areas (in two dimensions) over which addition rates and inferred fluxes can be calculated during chamber construction (3) or in a feeder system (4). Estimates, even in the same magma plumbing system, may be dramatically different if based on interpretation of the preserved plutonic record at these different settings. These local estimates can only be related to regional addition rate or volumetric flux calculations if assumptions are made about the relationship between the local and all other magma plumbing systems in the regional area.

MAGMATIC ADDITION RATES AND VOLUME FLUXES AS FUNCTIONS OF SCALE AND CRUSTAL DEPTH

Figure 9 displays crustal columns constructed from the two areas discussed above, plus the two other arc sections we are currently working on, and exemplifies the challenge of how to determine magma addition rates or volumetric fluxes in natural systems. The thermal modeling in the previous section (Figs. 10–14) emphasized that volumetric flux and spatial focusing are the dominant controls of thermal histories.

Figures 15 and 16 emphasize a number of challenges of calculating magma volume flux whether in natural systems or thermal models. What areas are chosen to determine addition rates or fluxes can dramatically affect the results: for example, in Figure 15 compare map slice 1 to 2 to local slices 3 and 4. Preserved plutonic material typically will be different in magnitude and composition in each (e.g., Fig. 9), and the relationship between the preserved plutonic material and former volumetric fluxes potentially dramatically different. Episodic magma systems and thermal models of these systems by their very nature have highly variable volumetric fluxes and resulting magma addition rates. We thus distinguish short-term versus averaged, long-term magma volumetric fluxes. Short-term magma fluxes depend on the volume, geometry, and ascent mechanism of an individual pulse; long-term magma fluxes depend on the scale and recurrence intervals of pulses, and thus our knowledge about them is dependent on the availability of high-precision geochronology. These may also vary as we consider volumetric fluxes in entire arcs versus single plutons and at different crustal depths (Figs. 9 and 15).

Equally problematic is determining the relationship between frozen magma systems and past volumetric fluxes in these systems. The simplest model (Fig. 16A), in which volume flux will be uniform no matter what part of the feeder system is examined, is probably not common in magmatic systems due to the thermal and mechanical drag effects of channel boundaries during flow (Fig. 16B). A second model including boundary effects is still probably inadequate for a typical rising pulse of magma, since it is likely that localized internal and return flow resulting in complex velocity gradients (Fig. 16C) may be a volumetrically important process (Saleeby, 1990; Farris and Paterson, 2007; Castro et al., 2008). In the most likely model, active magmatic systems are open, multiphase, and internally complex, and therefore processes such as host assimilation, internal crystal and melt differentiation, and mixing must be evaluated during both magma addition rate and volumetric flux calculations (Fig. 16D).

It is also important to return to the two end-member views of plutonic systems (Fig. 3): (1) that plutons represent an enclosed, trapped pulse of magma, or (2) that plutons represent frozen slices of a complex magma plumbing system. The latter may record some unclear, integrated time slice through a flowing, pulsating stream of magma with highly variable short-term fluxes that potentially can underestimate or overestimate long-term fluxes. Attempting to start from maps of slices through these systems (Fig. 17) and working backward to understand the 3-D nature of these systems to calculate volume addition rates (Figs. 3 and 9) and then the past volumetric fluxes of magma through these systems (Fig. 16) is a complicated undertaking and very dependent on assumed chamber growth models (Fig. 17).

Although rarely practical, the ideal goal would be to vertically integrate volumetric addition rates and magma volume flux calculations over an entire magma plumbing system, including erupted materials, since magma that moved through one part of system must have passed through deeper levels and then be either trapped higher in the system or have erupted. In all arc sections we have examined, magma addition

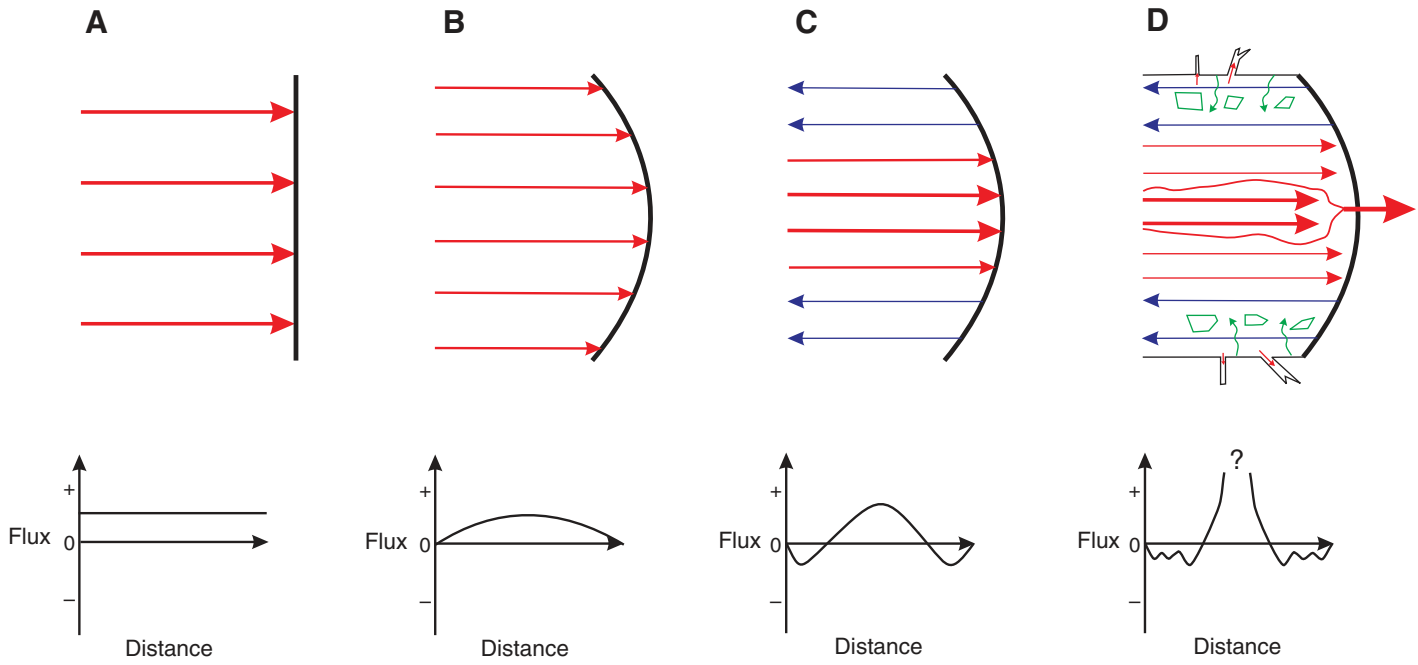

Figure 16. Schematic flow models that exemplify issues when calculating magma volumetric fluxes in magmatic systems. (A) Uniform flow gradient (arrows represent velocities) and resulting uniform calculated volumetric flux across a single flow channel. (B) Flow and calculated flux higher in the center of a single channel with decreasing flow gradient toward the margins. (C) Like B, except that the margins undergo return flow (blue) to help accommodate higher flow and flux in the center of the channel. (D) High flow and calculated flux in the center, but with many additional complexities at the margins, and flow out of the system. Complexities include return flow (blue), assimilation and stoping of host rock (green), and diking into the host rock, i.e., sideways flow, counteracting upward flow (red).

rates, particularly if integrated over the entire vertical column, increase drastically as more vertically extensive columns (deeper sections) are considered (i.e., the percent of preserved magmatism increases with depth, so integration of volumetric magma addition throughout the column must also). In the simplest possible sense (akin to a flow model in Fig. 16A), on the time scale of the entire ascent process, the long-term, volumetric flux through a horizontal area of a vertical channel, such as a dike, must also become greater with depth (since in this scenario the duration of the event and cross-sectional area of the feeder zone are assumed to be fixed) since it integrates the added volume of all magma that has continued to shallower levels plus what is trapped at the level of observation. Host-rock partial melting and assimilation, as well as the remobilization of scoured plutonic material, will affect the interpretation of these magma addition rates and inferred net flux at and above the level of integration. A scenario in which downward flow occurs during ascent, regardless of its cause, will reduce volumetric addition rates higher in the column and generate positive and negative volumetric fluxes across a plane, thus complicating the interpretation of net flux across the plane. Many processes such as crystal fractionation and the movement of smaller bodies within a plutonic system add complications to both volumetric addition rates and flux calculations and potentially reduce the true magma flux in the shallower portions of a system.

We present some initial magma addition rates and flux calculations at scales ranging from arc segments (Fig. 1) to individual plutons and at different crustal depths (Fig. 9) by combining data from our new field maps with new geochronology. We find it difficult to precisely compare these values to previous regional studies (Fig. 1) and in some cases our own thermal models (Figs. 10–14), since either complete information about the addition rates and flux issues is lacking (e.g., previous publications) or because of the challenges of considering 2-D models to poorly constrained 3-D natural systems in which the spatial distribution of addition rates and fluxes is also crucial. Furthermore, it is difficult to compare values of addition rates and volumetric fluxes from single, irregularly shaped magma plumbing systems (plutons) from regional values often normalized to arc kilometers (note that plutons are always narrower than complete arc widths). We thus urge caution in use of these addition rate and flux comparisons.

Sierra Nevada and TB Addition Rates and Fluxes

Since limited to currently exposed plutonic rocks, the apparent magma addition rates per arc length in the Sierra Nevada arc are ~10 km^3/m.y./km arc length; during the Cretaceous flare-up, when ~78% volume of magma was emplaced into the crust in only 15 m.y., this rate increased to ~85 km^3/m.y./km arc length (Ducea, 2001). In the southern Sierra Nevada, where the deepest parts of the Sierran arc are exposed, total addition rates during the Late Cretaceous flare-up have been estimated to be four times as high as modeled for oceanic-island arcs. For example, Saleeby et al. (2008) calculated for the Bear Valley suite a magma volume production rate of 22,500 km^3/m.y., which corresponds to an areal addition rate of ~5000 km^2/m.y. Ducea and Barton (2007) used CONTACT88 and NAVDAT databases to compare available addition rate variations with ε_{Nd} (and $^{87}Sr/^{86}Sr$) isotope data from the Sierra Nevada and adjacent batholiths, and concluded that the flare-ups are strongly correlated with Nd isotopic pull-downs toward more evolved compositions, whereas magma lulls are associated with Nd isotopic pull-ups. DeCelles et al. (2009)

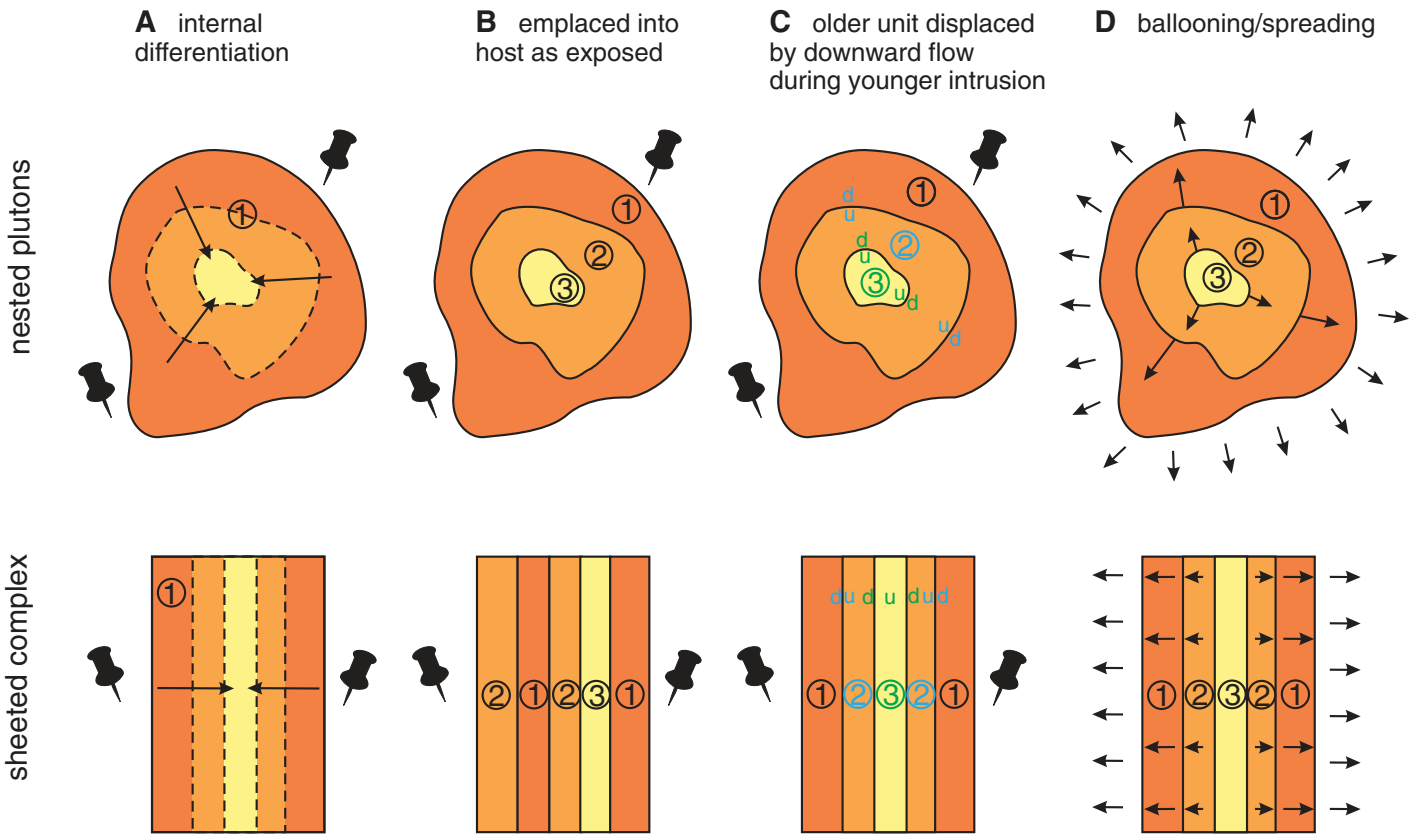

Figure 17. Examples of challenges of evaluating map patterns when calculating magma addition rates and inferred volumetric flux. Map patterns are of a concentrically zoned pluton and a sheeted complex. Both of these patterns can be formed by different processes, which complicate calculations, but need to be considered. (A) Pluton (in each example) intruded entirely as one pulse at stage one. Only inward differentiation and/or fractionation occur afterward. Pluton size does not change. (B) Pulses intrude into host in shape, position, and extent as exposed in three different stages. Host is incrementally being replaced by pluton material by vertical removal of host out of plan. No lateral expansion of host rock. (C) The first unit is emplaced in the extent of the entire pluton at stage one. As subsequent, younger units intrude, the older units (presumably magma mush) are vertically displaced through downward flow, e.g., in a nested diapir; d—down, u—up. (D) New pulses are emplaced into the center of the pluton while older pulses are displaced sideways straining host (including older pulses), and potentially also downward. Pushpins are locations of non-moving crust during magma chamber growth.

suggested that while the baseline magmatism is mostly derived from the mantle wedge, the high magma addition rate events are attributed to lithospheric underthrusting of the North American plate, from which as much as 50% of the arc magmatism was derived.

To estimate volumetric fluxes from these data is difficult for the following reasons: (1) map patterns are inherently biased toward the younger stages of batholith evolution (Fig. 17); (2) we don't know how much material has been transferred through the batholith to the surface; (3) we have little knowledge about the extent of the older units before being intruded by the next unit and thus how much previous material was displaced up or down out of the map section; and (4) even with dramatically increased geochronologic precision, it is difficult to estimate the time scales of local magmatic lulls between short episodes of magma surges into magma chambers (cf. Figs. 5 and 17).

Calculating addition rates and volumetric magma fluxes in a more localized setting such as the TB during its 10-m.y.-long growth has challenges and may vary tremendously depending on the selected chamber growth model. Volumetric fluxes will vary, depending on if, for example, one small, central dike is feeding the TB magma chamber in contrast to the present extent of the TB representing the former extent of a crustal magma pathway. We attempted to estimate magma volumes per million years for the TB and its individual units based on their areal distribution at the exposure level today, their estimated extent at depth, and their known U-Pb zircon ages (Coleman et al., 2004; Matzel et al., 2005, 2006b; Memeti et al., 2010). The TB occupies a map area of 1100 km^2 and ranges in age from 94.6 ± 0.3 Ma to 85.1 ± 0.9 Ma, thus spanning 9.5 m.y. of crystallization history. The continuation of the Tuolumne intrusion at depth probably varies between 1.5 km for the Johnson Peak granite (Titus et al., 2005) and 5–10 km or possibly greater for the main part of the TB (Oliver et al., 1988; Bateman, 1992; Saleeby et al., 2003, 2008). If the geometry of the TB, with a horizontal extent as large as the area exposed today and a minimum vertical extent of 5 km, is correct, the minimum magma addition rate at the emplacement level of the TB yields ~580 km^3/m.y. (for 5 km pluton depth). This estimate considers the magma volume emplaced over the entire time the TB was active.

We suggest that the Cathedral Peak granite (the youngest major TB unit), the Johnson Peak porphyry (the smallest body in the center), and the peripheral lobes most likely were

as extensive as their current preserved areas of exposure during construction of the TB. These units thus may give us the most realistic estimates for magma addition rates in the TB over smaller time scales (1–2 m.y.). In contrast, the older Kuna Crest or the Half Dome units may have occupied the entire area of the TB before the Cathedral Peak intruded into that space, but then were vertically displaced (up or down) due to the subsequent emplacement of the younger TB units in the center (Fig. 17). Thus using the current exposed area of the Kuna Crest and the Half Dome units on the geologic map (Huber et al., 1989) gives us magma volume addition rate estimates with greater uncertainty and values that may be too low.

If we accept this assessment, possible magma addition rates can be bracketed by assuming unit thicknesses of 1, 5, or 10 km and using different growth models that will result in maximum or minimum rates (Fig. 18). Minimum magma addition rates are ~285 km^3/m.y. for the Kuna Crest granodiorite, ~660 km^3/m.y. for the Half Dome Granodiorite, 970 km^3/m.y. for the Cathedral Peak granite (extending ~5 km into depth; Oliver et al., 1988), and 17 km^3/m.y. for the Johnson Peak granite (using 1.5 km depth; Titus et al., 2005), and range for the different 10–60 km^2 lobes from 10 to 40 km^3/m.y. for 1 km depth to 50–200 km^3/m.y. for 5 km vertical extent (Fig. 18). Although these calculations are just rough estimates, they show that the magma addition rate overall was mostly less than 1000 km^3/m.y. (over an area of a single batholith). Furthermore, these calculations suggest that the magma addition rate per 1 m.y. over the entire time of the construction of the TB is lower than the magma addition rate calculated for the shorter lived Cathedral Peak unit (2 m.y. versus 10 m.y.). These results suggest that magma addition into the emplacement level was episodic and that volumes may have been much higher over shorter periods of time (flare-ups), which were separated by lulls in magmatism; a conclusion we reach independently with the lobe studies.

If we assume particular end-member emplacement scenarios (used to decide the 2-D area of feeder zones through which the magma passed), these data can be used to explore a potential range of volumetric fluxes. If we assume that magma only ascended (no return flow) through a 10 m^2 dike-like channel versus through a 10 km^2 diapir-like channel, and taking the maximum (970 km^3/m.y.) and minimum (17 km^3/m.y.) estimated magma addition rates, we get a range of volumetric flux rates from 1.7 km^3/km^2/m.y (smallest addition rate through largest feeder zone) to 9.7×10^4 km^3/km^2/m.y (largest addition rate through smallest dike-like feeder zone). We suspect that these are minimum fluxes in some cases due to issues (discussed herein). However, it is clear that a huge range of volumetric flux rates probably occurred in these single magma plumbing systems.

Cascades Core Addition Rates and Volume Fluxes

The compilation of pluton areas, combined with geochronological data, enables determination of minimum magma addition rates during construction of the Cretaceous Cascades arc, although we are faced with the same challenges as discussed previously herein. Minimum addition rates were estimated by multiplying the pluton area times the average topographic relief, which is ≥1.6 km. These calculations indicate that the greatest addition of magma in the crustal column and adjacent parts of the Cascades core occurred between 96 and 89 Ma (Fig. 1). A minimum of 3586 km^3 of magma intruded over an arc length of 130 km, the length for which there is reasonable geochronological

Figure 18. Histograms of estimated volume addition rates for the Tuolumne batholith (TB). HD—Half Dome Granodiorite (eHD—equigranular; pHD—porphyritic), CP—Cathedral Peak Granodiorite and/or granite, KC—Kuna Crest granodiorite. (A) Using inferred areal extent of units prior to intrusion of younger units, which then removed portions of earlier phases (probable maximum [max] estimates). (B) Using present-day areal distributions (probable minimum [min] estimates). In both cases durations of growth of units (listed in parentheses) were based on the range of zircon ages in each unit determined from our new chemical abrasion–thermal ionization mass spectrometry zircon dating (e.g., Memeti et al., 2010), contacts were assumed to be vertical, and units were assumed to be either 1, 5, or 10 km thick.

control in the Cascades core. This corresponds to an average minimum volume addition rate of 512 km^3/m.y. or volume addition rate per arc length of 3.9 km^3/m.y./arc-km during this 7 m.y. interval. Assuming more realistic thicknesses of 5 km (still probably an underestimate), then values of magma volume addition rates of 1.6×10^3 km^3/m.y. volume addition rate per arc length and 12 km^3/m.y./arc-km are obtained. Higher rates likely occurred over shorter time periods. Matzel et al. (2006a) calculated a minimum volume addition rate of 3.1×10^3 km^3/m.y. during the maximum 300 k.y. construction of the 91 Ma phase (~208 km^2) of the Mount Stuart batholith (Fig. 19).

There was little magmatism between 88 and 79 Ma, and the other significant pulse of Cretaceous plutonism was from ca. 78 to 71 Ma (Fig. 1). Dated plutons from the latter age interval crystallized in the deep to mid-crust (6–8 kbar). A minimum of 750 km^3 of magma was intruded, resulting in an average minimum addition rate of 0.8 km^3/m.y./km of arc length assuming a thickness of 1.6 km, and 2.6 km^3/m.y./km of arc length assuming a thickness of 5 km. These addition rates are <25% of those from 96 to 89 Ma, and indicate that the greatest magmatic addition rate occurred during the peak of regional mid-Cretaceous shortening of the Coast belt. Reduced magmatism from 88 to 71 Ma was synchronous with an interval of inferred regional transpression (Miller and Bowring, 1990; Hurlow, 1992). We did not extend this analysis to younger time intervals, as the major locus of Eocene magmatism is northeast of the crustal column (Haugerud et al., 1991), and crystallization ages of protoliths of large volumes of orthogneiss in the Skagit Gneiss Complex are poorly known.

Estimates of magma addition rates and inferred fluxes can also be made for two individual plumbing systems, or plutons, as well (Fig. 19). Using our previous mapping and the high-precision U-Pb zircon ages for the Mount Stuart and Tenpeak plutons (Matzel et al., 2006a), estimates of volume addition rates through time can be calculated using the same approach as discussed herein for the TB (Fig. 19B). As noted by Matzel et al. (2006a), volume addition rates appear to have been more episodic in the Mount Stuart pluton (estimates range to 1000 km^3/m.y.), whereas the Tenpeak pluton appears to have had a more continuous construction (average volume addition rate of ~400 km^3/m.y).

The estimated volume addition rates for the North Cascades are broadly similar to, or lower than, those calculated for other arcs. For example, Francis and Rundle (1976) reported values of 2.9 km^3/m.y./arc-km for the Peruvian Coastal Batholith and 8.9 km^3/m.y./arc-km for the Cordillera Blanca batholith, assuming average pluton thicknesses of 5 km. As discussed herein, the apparent long-term magma addition rate to the Sierra Nevada Batholith is ~10 km^3/m.y./arc-km and, during the major Cretaceous flare-up in the batholith, the rate reached 85 km^3/m.y./arc-km (Ducea, 2001).

If we make the same assumptions as for the Sierra Nevada (i.e., 10 m^2 dike-like channels and 10 km^2 diapir-like channels and no return flow), we get a range of volumetric flux rates for the Cascades systems that are as high as 3.1×10^5 km^3/km^2/m.y. For individual plutons like the Mount Stuart and Tenpeak, making the same assumptions about the size of feeder zones, potential fluxes can range from nearly 0 to 10^5 km^3/km^2/m.y. (Figs. 2 and 19).

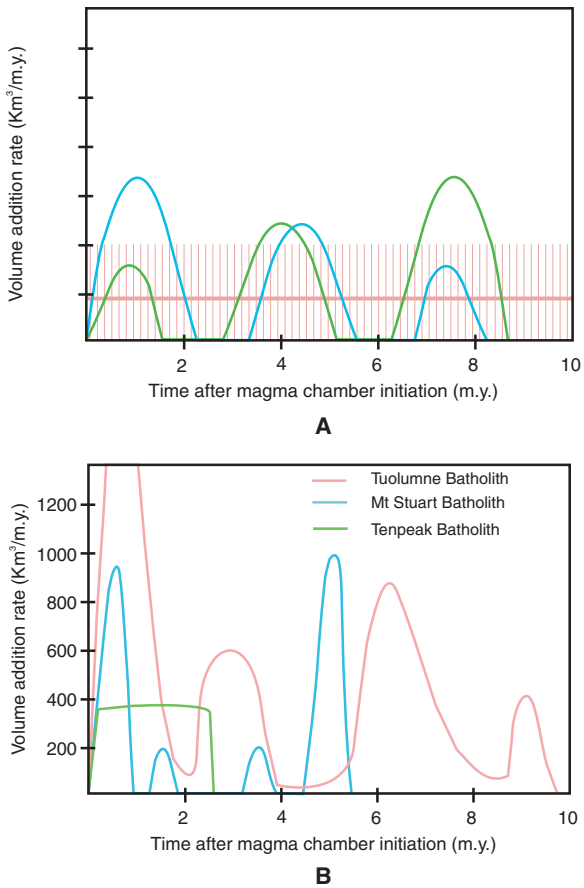

Figure 19. (A) Hypothetical plots of magma volume addition rates (VAR) versus time in plutons. (B) Estimated plots. In A, vertical red lines show short-duration VARS during dike emplacement separated by periods of no magma addition; thicker horizontal red line is long-term VAR average of dike emplacement. Exact horizontal position of line will depend on dike size and temporal spacing. This horizontal red line could also represent constant slow addition of magma to a chamber. Green and blue curves show possible models of episodic growth of chambers through addition of larger magma pulses and/or nonsteady-state flow of magma into a chamber. Blue is first pulse, the biggest and nesting of subsequent pulses. Green pulse size or total amount fed into chamber grows through time and extends beyond earlier margins.

DISCUSSION

As the precision and number of geochronologic studies of oceanic and continental margin arc magmatism have increased (Gehrels et al., 2009; Barth et al., 2008), it has been well established that long-term, regional, magmatic volume addition rates vary dramatically in these arcs and that there is a pattern, or tempo, to the periods of these high and low addition rates (Fig. 1). Detailed studies of more localized tilted portions of some of these same arcs (Fig. 9) provide ample evidence that during active magmatism a huge range of magma pulse sizes and shapes existed at all crustal levels, and that the total volume of trapped magmatic material typically increased with depth (Miller and Snoke, 2009). Thus these I-type (igneous protolith) dominated systems are dramatically different than the S-type (sedimentary protolith) systems examined by other workers, such as the models of Annen et al. (2006a, 2006b).

It remains difficult in these higher magma volume Cordilleran type arcs to determine a more detailed record of the size and recurrence intervals between individual pulses, although the presence of both strongly sheeted bodies and more homogeneous bodies with gradual internal changes of compositions and structures suggests that a wide range of pulse sizes, recurrence intervals, and resulting magma chambers likely occurred (Figs. 9 and 19). Thus one of the challenges in evaluating the episodic evolution of these arc systems is to develop criteria for recognizing individual magma pulses and to establish both their internal history and the degree to which they differ from and interact with adjacent pulses. This may be particularly

challenging in apparently homogeneous plutons constructed of smaller pulses that some have argued are now bounded by cryptic contacts (Coleman et al., 2005).

In Vernon and Paterson (2007) it was noted that there are three common types of internal boundaries in granitoids (Figs. 6 and 8), defined by: (1) distinct compositions, (2) same compositions, but different microstructures, and (3) identical compositions and microstructures; type 3 was argued to be uncommon, since most contacts are marked by (1) slight microstructural variations if the juxtaposed magmas were at two different temperatures, (2) slight modal changes in minerals, possibly due to flow sorting (Barrière, 1981), and/or (3) the presence of enclaves or pieces of host rock trapped along the contact (Miller and Paterson, 2001a). An additional complication is that these three types of internal boundaries may form by other processes, besides the addition of new pulses into a chamber, such as localized flow of magma within a chamber, and by processes during crystallization, such as crystal-liquid fractionation. It was suggested (Vernon and Paterson, 2007) that some progress can be made in testing these alternatives using field and microstructural observations by determining (1) whether internal contacts, or gradations in composition between contacts or gradations in magmatic microstructures between contacts, are preserved in a pluton; (2) whether these features are laterally continuous or gradually disappear along strike; and (3) whether magmatic foliations and lineations defined by the alignment of minerals with magmatic microstructures overprint or are cut by the contacts. Ultimately it would be helpful to establish further tools, such as a statistically determined geochemical index of diversity that defines the geochemical breadth of compositional diversity possible in a single pulse, as compared to genetically distinct pulses, or those that formed locally.

It is likely that many larger, more homogeneous plutonic bodies are made up of separate pulses. However, our studies of a range of plutons with different compositions and at different crustal depths indicate that many incrementally grown systems typically preserve evidence of the pulse sizes trapped in chambers through preservation of internal contacts between pulses (e.g., Pitcher and Berger, 1972). For example, in the Cascades area, extensively sheeted, mid-crustal (~6–7 kbar) tonalitic plutons in the Cascades core were described (Miller and Paterson, 2001a), in which (1) internal contacts are readily apparent, (2) disaggregated and locally rotated enclaves (xenoliths and microgranitoid enclaves) occur along the contacts, and (3) microstructural observations show very little evidence of intergranular changes that might aid in removing evidence of these contacts (Vernon and Paterson, 2007). Thus, even in these deeper and hotter plutons, internal contacts are well preserved, and are continuous over hundreds of meters to kilometers, even between sheets with fairly similar compositions (Fig. 8).

Cryptic contacts between separate pulses are more likely to form as the juxtaposed magmas become compositionally similar and/or as melt contents in both pulses increase. However, in these cases one can suggest that the recognition of different pulses is of less importance in regard to questions about magma fluxes and chamber sizes. For example, a reexamination of likely magma flow in complex plumbing systems, such as those in Figures 3, 9, 16, and 17, makes it likely that closely related magmas may at times separate and recombine as they move up through these systems and at times form continuous magma bodies.

In summary, we see ample evidence that laterally extensive internal structures that define pulse boundaries are typically well preserved at all crustal levels and with careful study can usually be distinguished from laterally discontinuous internal contacts formed by processes within already constructed chambers (Paterson et al., 2008; Žák et al., 2009). For plutons in which internal compositions and magmatic structures vary gradually, and laterally continuous internal contacts are not readily visible, we suggest that in situ incremental growth is unlikely, and alternatively that these zones represent either large pulses that have internally differentiated, or that extensive mixing and partial homogenization followed the earlier incremental growth of these large pulses.

An additional challenge in recognizing pulses and establishing pulse histories is the increased documentation that magma batches often have a complex cargo of crystals with distinct histories. For example, Davidson et al. (1998, 2005, 2007) and others (Christensen et al., 1995; Hoskin et al., 1998; Costa et al., 2003; Barbey et al., 2005; Ramos and Reid, 2005; Gagnevin et al., 2005; Wallace and Bergantz, 2005; Morgan et al., 2007) demonstrated, using isotopic fingerprinting in single minerals, that crystal exchange between different liquids is a common phenomenon and that the resulting crystal populations of both volcanic and plutonic suites are often cargoes accumulated from two or more sources. Recent high-precision U-Pb TIMS zircon dating of multiple, single grains supports this conclusion through the recognition that zircon populations are also a mix of xenocrysts, antecrysts, and autocrysts (e.g., Brown and Fletcher, 1999; Charlier et al., 2005; Bindeman et al., 2008; Matzel et al., 2006b; Miller et al., 2007; Memeti et al., 2010). The resultant volcanic or plutonic rock is thus a mechanical mixture of crystals, which requires that extensive mixing occurred between pulses, that crystals were plucked from stalled crystal mush zones by an ascending pulse, or that some poorly understood processes occurred within pulses that affect geochemistry and/or age of crystals. This clear signal of crystal mixing implies that the mixing process may further muddy the record and/or recognition of individual pulses.

Our thermal modeling of a large range of incremental growth scenarios suggested by our field studies strongly indicates that the overall behavior of these systems, and specifically how large and long-lived magma chambers were, is very dependent on the spatial distribution and/or extent of short- and long-term volumetric fluxes, the long-term rates being a function of pulse size and recurrence interval (Fig. 2). In our thermal models the pulse size, pulse recurrence, and pulse clustering had primary effects on resulting chamber size and durations, whereas the magma and host-rock properties and pulse shape had important, but secondary effects (Figs. 10–14). Our thermal modeling also indicates that there are many geologically reasonable scenarios in which large and long-lived chambers can form by the incremental addition of small pulses over durations as short as 50–100 k.y. at middle and upper crustal levels (e.g., Yoshinobu et al., 1998) and even faster at deeper levels, resulting in magma chambers with long hypersolidus histories in the range of 0.5 to >1 m.y. (Figs. 2 and 10–14).

We infer that the degree to which larger and longer duration magma chambers form will naturally influence the degree to which internal differentiation, convection, and mixing processes operate in these systems, as well as the controls on volcanic eruptions and the thermal and/or rheological effects on the surrounding host rocks. It is also intriguing to speculate that the incremental addition of magma pulses over longer durations in magma chambers will aid in diapiric ascent through maintaining a higher heat budget in these large, buoyant magma bodies (e.g., Marsh, 1982; Paterson and Vernon, 1995).

If one keeps in mind the assumptions needed to proceed, then it is possible to compare our estimates of magma volume addition rates and volumetric fluxes determined from natural arc sections to our better constrained addition rates and fluxes in the thermal models. We find that there is significant overlap and some intriguing correlations. In magmatic systems (thus ignoring the higher fluxes in large, short-duration volcanic eruptions) magma surges typically have long-term volumetric fluxes ranging between

10^3 and 10^5 km^3/km^2/m.y. (Fig. 2), values compatible with values for our thermal modeling of large nested pulses (vertical cylinders, or nested disk-shaped bodies). In these cases large chambers form rapidly and have durations (at least at their centers) of >1 m.y. and sometimes >2 m.y. In contrast, more normal background magmatic activity results in volumetric fluxes ranging between 10^1 and 10^3 km^3/km^2/m.y. (Fig. 2), values compatible with our thermal modeling of smaller sheeted to irregular shaped pulses or less focused magmatic systems. In these cases magma chambers can still grow, but tend to be more ephemeral and have durations no greater than 0.5 m.y. Magmatic lulls have even lower long-term volumetric fluxes and thus smaller and/or shorter duration chambers.

The importance of magma fluxes, and equally the degree of clustering of magma pulses, which can be thought of in terms of spatial focusing of addition rates or volume fluxes, draws attention to the need for a much larger and more robust data set on both magma addition rates and ideally volumetric fluxes. Unfortunately, it also draws attention to the very difficult challenges faced in trying to obtain robust estimates. We have raised a number of issues that arise when trying to relate flux measurements in even fairly simple flow systems (Fig. 16) to fairly simple map patterns (Fig. 17), even if high-precision geochronology is available, that further increase in complexity when trying to relate these map patterns to natural, fully 3-D magma plumbing systems (Figs. 5–9, 15, and 19). Minimum estimates of volumetric magma addition to local crustal levels in arcs are often quoted in papers (see citations herein), but without having better 3-D information about magma pathways, whether additional magma passes up (volcanic eruptions) or down (magma return flow during rise of younger pulses) through the system, and the degree to which internal differentiation and contamination affected these systems, robust volumetric fluxes and temporal and/or spatial variations in fluxes will remain elusive.

An exciting future direction of research on magmatic systems will be to better constrain the former history of magma movement through former magma plumbing systems. Figure 19 is our preliminary attempt to address some of these issues. Figure 19A displays some theoretical patterns of volume addition rates versus time for different types of magma chamber construction models and Figure 19B shows estimates of what these patterns look like in the three plutons discussed, for which detailed mapping and high-precision geochronology are available. None of the plutons show the same pattern, although at least two of the three appear to be episodically constructed. Episodic magmatism in these systems leads us to question why it is episodic, and whether there are temporal and spatial patterns to this episodicity. If so, is there a tempo in single plumbing systems comparable to that suggested from regional studies of arc magmatism, orogeny, and erosion (cf. Figs. 1 and 19)? Is this tempo largely a function of source melting processes, feedback processes within the magmatic plumbing system, or some form of external forcing? Clearly the assumptions made in constructing Figure 19B need to be further tested and additional plutons studies need to be added before we can realistically address these questions.

CONCLUSIONS

In continental margin arcs, the incremental growth of plutonic bodies is common and reflects the complex movement of magma through irregularly shaped magma plumbing systems.

Exposures of single plutons provide cross sections through vertical plumbing systems that often record a complex history of construction and growth over durations ranging to ~10 m.y.

Incremental growth results in both focused and unfocused magmatic systems, the former often resulting in larger, compositionally zoned plutons, many with early sheeting along their margins. This incremental, longer duration addition of heat in focused systems may enhance convection, mixing, and fractionation in chambers and the number and lifespans of diapiric bodies.

Unfocused systems result in migmatite terrains, no large chambers, and accompanying processes of convection and in situ mixing, and less well constrained growth durations.

The resulting crustal columns display a large range in the size and shape of plutonic bodies, each made up of a variable number of internal pulses, and in all cases show an increase of plutonic material with crustal depth, typically reaching values of >65% plutonic material in the lower crust.

Finite difference thermal models of a wide range of incremental growth scenarios of focused magma systems indicate that magma chambers can form in 50–100 k.y. and subsequently continue to grow to sizes much greater than individual pulses, and have durations of <0.5 to >1 m.y.

Estimates of long-term magma addition rates in arcs range from near zero during magmatic lulls to ≥900 km^3/m.y. during magmatic flare-ups. Magma addition rates in single plumbing systems range to 3×10^5 km^3/m.y. (Cascades) and 9.7×10^3 km^3/m.y. (Sierra).

If certain emplacement models (or areal sizes of feeder zones) are assumed, then volumetric magmatic fluxes can be estimated for natural systems. These range between 10^3 and 10^5 km^3/km^2/m.y. during magmatic surges, values compatible with our thermal modeling of large nested pulses (vertical cylinders, or nested disk-shaped bodies), to between 10^1 and 10^3 km^3/km^2/m.y. in more normal magmatic episodes, values compatible with our thermal modeling of smaller sheeted to irregularly shaped pulses and less focused magmatic systems.

In the magmatic surge cases, large chambers form rapidly and have durations (at least in their centers) of >1 m.y. and sometimes >2 m.y. In the latter case chambers are highly ephemeral and have durations no greater than 0.5 m.y.

A number of challenges remain in recognizing far-traveled versus locally formed pulses, establishing internal pulse histories, pulse recurrence intervals, and short- and long-term magma fluxes, and thus if the tempo seen at arc scales also occurs at the scale of individual magma plumbing systems.

APPENDIX

TABLE A1. DEFINITIONS USED IN THIS PAPER IN COMPARISON TO DEFINITIONS USED BY OTHERS

Quantity	Units	Sometimes referred to as
Total added volume	km^3	magma addition
Volume addition rate	km^3/m.y.	magma flux; magma addition rate
Volumetric magmatic flux	km^3/km^2/m.y. = km/m.y.	
Areal addition rate	km^2/m.y.	
Volume addition rate per arc length	(km^3/m.y.)/(arc-km)	apparent intrusive flux; Armstrong unit; magma addition rate

TABLE A2. PARAMETERS FOR THERMAL MODELS SHOWN IN FIGURES 10–14

	Parameter	Units	Figure 10 panel A	Figure 10 panel B	Figure 10 panel C	Figure 10 panel D	Figure 11	Figure 12 panel A	Figure 12 panel B	Figure 12 panel C	Figure 13	Figure 14
Category			dikes	sills	dikes & sills	blobs	incremental expansion	40 km-wide sequence	10-km wide	many small -> 40,30,20,5 km	mapped pluton shapes	pluton cross section
Host rock	type		amphibolite				granodiorite	granodiorite			same as	same as
	initial temperature	°C	300				0	300			Fig. 11	Fig. 11
	density	kg/m^3	3000				2700	2700			:	:
	thermal conductivity	W/m °K	3.15				2.65	2.65			:	:
	specific heat	J/kg °K	1142				1142	1142			:	:
	latent heat of fusion	J/mole	220,000				150,000	150,000			:	:
	l.h.o.f. release temp.	°C	725				725	725			:	:
	radiogenic	W/m^3	—				—	—			—	6.5×10^{-6}
	radiogenic depths	km	—				—	—			—	0–15 km
Intrusion rock	type		granodiorite				diorite	four pulses: 1 = diorite; 2–3 = granodiorite; 4=granite			same as	same as
	temperature	°C	800				900	900 – 850 – 850 – 775			Fig. 11	Fig. 11
	density	kg/m^3	2700				2800	2800 – 2700 – 2700 – 2670			:	:
	thermal conductivity	W/m °K	3.05				2.65	2.65 – 2.65 – 2.65 – 3.05			:	:
	specific heat	J/kg °K	1142				1142	1142 – 1142 – 1142 – 1000			:	:
	latent heat of fusion	J/mole	150,000				150,000	all 150,000			:	:
	l.h.o.f. release temp.	°C	650				750	750 – 725 – 725 – 675			:	:
Intrusion process	description		episodic (many small)				incremental	each all-at-once		incremental	map shapes	map disk
	time per intrusion	varies	250 years				2500 yrs	0, 3, 6, 9 My		2.5, 3.3, 5, 20 ky	0, 2, 6, 6.5 My	same as Fig. 12
	duration of intrusions	varies	100,000 years				400,000 yrs	instantaneous		1 My each	instantaneous	instantaneous
	region Xmin	km	7.5	0			emplaced @10 km					
	region Xmax	km	15	20			expands to 26 km					
	region Zmin	km	0	7.5			5					
	region Zmax	km	20	15			15					
	random placement-X		bounded	Gaussian				centered				
	random placement-Z		Gaussian	bounded				centered				
	shape		rectangular		elliptical		rectangular	rectangular				
	orientation		vertical	horizontal	both		vertical					
	max individual length	km	5			2	0.1	40, 30, 20, 5 wide	10, 6, 8, 4	0.1		
	max individual height	km	0.5			2	10					
	random aspect ratio		gaussian									
Model size	length (X)	km	20				40	200			165 (E-W)	62 (E-W)
	depth (Z)	km	20				40	60			165 (N-S)	30 (depth)
	grid spacing	km	0.02				0.1	0.1			0.2063	0.2063
Model time	total duration	My	0.1				0.4	15			10	10
	calculation step	years	3.5				92	91			250	250
	″ ″	sec	1.01×10^9				2.91×10^8	2.91×10^9			1.58×10^{13}	1.58×10^{13}
Model setup	initial conditions		constant (300 °C)				geothermal	constant (300 °C)			constant (300 °C)	geothermal
	boundary conditions		absorbing				gradient	absorbing			constant (300 °C)	gradient
Computation	#time steps		31,197				4,775	163,614			44,001	122,001
	computer memory	Mbytes	56				10	68			26	3

Note: These parameters describe modeling rock properties, initial and boundary conditions, intrusion geometries and rates, and computation resources.

TABLE A3. CALCULATION OF MAGMA ADDITION RATES AND VOLUMETRIC FLUXES FOR THERMAL MODELS SHOWN IN FIGURES 10–14

		2D dim.	Event	Total added volume (km²)	Duration (yr)	2D Volume addition rate (km²/my)	Intrusive surface area *(just X if x-z)* (km)	2D Vol. flux (km²/km/my = km/my)	Width (km): 1.00	3D Total added volume (km³)	Duration (yr)	3D Volume addition rate (km³/my)	Intrusive surface area (km²)	3D Volumetric flux (km³/km²/my = km/my)
Figure 10 (four panels)	A	x-z	all	259.8	100,000	2.60E+03	7.5	3.46E+02		259.8	100,000	2.60E+03	7.5	3.46E+02
	B	x-z	all	261.3	100,000	2.61E+03	20	1.31E+02		261.3	100,000	2.61E+03	20.0	1.31E+02
	C	x-z	all	227.2	100,000	2.27E+03	20	1.14E+02		227.2	100,000	2.27E+03	20.0	1.14E+02
	D	x-z	all	363.5	100,000	3.64E+03	20	1.82E+02		363.5	100,000	3.64E+03	20.0	1.82E+02
Figure 11 expanding reservoir		x-z	all	160	400,000	4.00E+02	feeder: 0.1	4.00E+03		160.0	400,000	4.00E+02	0.1	4.00E+03
							whole zone: 16	2.50E+01		160.0	400,000	4.00E+02	16.0	2.50E+01

		2D dim.	Event radius (km)	2D Total added volume (km²)	Duration (instantan. – use 1 calc. time step) (yr)	2D Volume addition rate (km²/my)	Intrusive surface area (km²)	2D Vol. flux (km²/km/my = km/my)	Height (km): 10.00	3D Total added volume (km³)	Duration (yr)	3D Volume addition rate (km³/my)	Intrusive surface area (km²)	3D Volumetric flux (km³/km²/my = km/my)
Figure 12 cylinders	A	x-y	40	5,026.5	91	5.52E+07	5,026.5	1.10E+04		50,265.5	91	5.52E+08	5,026.5	1.10E+05
			30	2,827.4	91	3.11E+07	2,827.4	1.10E+04		28,274.3	91	3.11E+08	2,827.4	1.10E+05
			20	1,256.6	91	1.38E+07	1,256.6	1.10E+04		12,566.4	91	1.38E+08	1,256.6	1.10E+05
			5	78.5	91	8.63E+05	78.5	1.10E+04		785.4	91	8.63E+06	78.5	1.10E+05
			sum	9,189.2	364	2.52E+07	9,189.2	2.75E+03		91,891.6	364	2.52E+08	9,189.2	2.75E+04
	B	x-y	10	314.2	91	3.45E+06	314.2	1.10E+04		3,141.6	91	3.45E+07	314.2	1.10E+05
			8	201.1	91	2.21E+06	201.1	1.10E+04		2,010.6	91	2.21E+07	201.1	1.10E+05
			6	113.1	91	1.24E+06	113.1	1.10E+04		1,131.0	91	1.24E+07	113.1	1.10E+05
			4	50.3	91	5.52E+05	50.3	1.10E+04		502.7	91	5.52E+06	50.3	1.10E+05
			sum	678.6	364	1.86E+06	678.6	2.75E+03		6,785.8	364	1.86E+07	678.6	2.75E+04
	C	x-y	40	5,026.5	1,000,000	5.03E+03	5,026.5	1.00E+00		50,265.5	1,000,000	5.03E+04	5,026.5	1.00E+01
			30	2,827.4	1,000,000	2.83E+03	2,827.4	1.00E+00		28,274.3	1,000,000	2.83E+04	2,827.4	1.00E+01
			20	1,256.6	1,000,000	1.26E+03	1,256.6	1.00E+00		12,566.4	1,000,000	1.26E+04	1,256.6	1.00E+01
			5	78.5	1,000,000	7.85E+01	78.5	1.00E+00		785.4	1,000,000	7.85E+02	78.5	1.00E+01
			sum	9,189.2	4,000,000	2.30E+03	9,189.2	2.50E-01		91,891.6	4,000,000	2.30E+04	9,189.2	2.50E+00

	Dim.	Event #	2D Total added volume (km²)	Duration (instantan. – use 1 calc. time step) (yr)	2D Volume addition rate (km²/my)	Intrusive surface area (km²)	2D Vol. flux (km²/km/my = km/my)	Height (km): 10.00	3D Total added volume (km³)	Duration (yr)	3D Volume addition rate (km³/my)	Intrusive surface area (km²)	3D Volumetric flux (km³/km²/my = km/my)
Figures 13–14 Tuolumne plutons	x-y	1	8,680.5	250	3.47E+07	8,680.5	4.00E+03		86,805.0	250	3.47E+08	8,680.5	4.00E+04
		2	7,473.9	250	2.99E+07	7,473.9	4.00E+03		74,739.0	250	2.99E+08	7,473.9	4.00E+04
		3	5,791.1	250	2.32E+07	5,791.1	4.00E+03		57,911.0	250	2.32E+08	5,791.1	4.00E+04
		4	163.0	250	6.52E+05	163.0	4.00E+03		1,630.0	250	6.52E+06	163.0	4.00E+04
		sum	22,108.5	1000	2.21E+07	22,108.5	1.00E+03		221,085.0	1000	2.21E+08	22,108.5	1.00E+04

Note: Because the modeling was performed in 2D (cross-sectional or map-view), the left side of this table computes area addition rates and fluxes. On the right side of the table, three-dimensional sizes of intrusions are defined, allowing for the calculation of 3D volumetric addition rates and fluxes. For the cross-sectional models in Figure 10, 2D area flux and the 3D volumetric flux have the same values. For the expanding reservoir in Figure 11, the flux can be calculated based on two different reference regions—the feeder zone or the area of the final reservoir size. The volumetric flux based solely on the feeder zone is 160 times greater than that based on the final reservoir size due to the feeder being a narrow but fixed location. In Figure 12, there is no fixed definition in the computer modeling of the amount of time required to emplace an "instantaneous intrusion." The longest amount of time is the time represented by one calculation time step. The addition rates and fluxes are calculated using this time step and hence represent lower values of the modeled instantaneous rates. This assumption is also applied to Figures 13–14. For the 3D volumetric calculations in Figures 12–14, the map-view intrusions are considered to be 10 km tall in the vertical direction.

ACKNOWLEDGMENTS

We thank two anonymous reviewers for useful reviews and Carol Frost and Francesco Mazzarini for editorial assistance. Paterson acknowledges support from National Science Foundation (NSF) grants EAR-0537892 and EAR-0073943. Miller acknowledges support from NSF grants EAR-9980662, EAR-0074099, and EAR-0511062. Paterson and Memeti are grateful for three years of financial support through the U.S. Geological Survey EDMAP program. Numerical modeling was performed using the University of Southern California (USC) geophysics computational facilities. We thank Adam Ianno for help on figure drafting, and acknowledge numerous USC graduate and undergraduate students for their assistance during field work and Yosemite National Park rangers for their constant support and interest in our work.

REFERENCES CITED

Adam, C., Vidal, V., and Escartin, J., 2007, 80-Myr history of buoyancy and volcanic fluxes along the trails of the Walvis and St. Helena hotspots (South Atlantic): Earth and Planetary Science Letters, v. 261, p. 432–442, doi: 10.1016/j.epsl.2007.07.005.

Ague, J.J., and Brimhall, G.H., 1988, Magmatic arc asymmetry and distribution of anomalous plutonic belts in the batholiths of California; effects of assimilation, crustal thickness, and depth of crystallization: Geological Society of America Bulletin, v. 100, p. 912–927, doi: 10.1130/0016-7606(1988)100<0912:MAAADO>2.3.CO;2.

Anderson, J.L., ed., 1990, The nature and origin of Cordilleran magmatism: Geological Society of America Memoir 174, 405 p.

Annen, C., Blundy, J., and Sparks, R.S.J., 2006a, The sources of granitic melt in deep hot zones: Royal Society of Edinburgh Transactions, Earth and Environmental Science, v. 97, p. 297–309, doi: 10.1017/s0263593300001462.

Annen, C., Scaillet, B., and Sparks, R.S.J., 2006b, Thermal constraints on the emplacement rate of a large intrusive complex: The Manaslu leucogranite, Nepal Himalaya: Journal of Petrology, v. 47, p. 71–95, doi: 10.1093/petrology/egi068.

Bacon, C.R., and Lanphere, M.A., 2006, Eruptive history and geochronology of Mount Mazama and the Crater Lake region, Oregon: Geological Society of America Bulletin, v. 118, p. 1331–1359, doi: 10.1130/B25906.1.

Bacon, C.R., and Lowenstern, J.B., 2005, Late Pleistocene granodiorite source for recycled zircon and phenocrysts in rhyodacite lava at Crater Lake, Oregon: Earth and Planetary Science Letters, v. 233, p. 277–293, doi: 10.1016/j.epsl.2005.02.012.

Barbey, P., Dereje, A., and Yirgu, G., 2005, Insight into the origin of gabbro-dioritic cumulophyric aggregates from silicic ignimbrites: Sr and Ba zoning profiles of plagioclase phenocrysts from Oligocene Ethiopian Plateau rhyolites: Contributions to Mineralogy and Petrology, v. 149, p. 233–245, doi: 10.1007/s00410-004-0647-2.

Barrière, M., 1981, On curved laminae, graded layers, convection currents and dynamic crystal sorting in the Ploumanc'h (Brittany) subalkaline granite: Contributions to Mineralogy and Petrology, v. 77, p. 214–224, doi: 10.1007/BF00373537.

Barth, A.P., Tosdal, R.M., Wooden, J.L., and Howard, K.A., 1997, Triassic plutonism in southern California: Southward younging of arc initiation along a truncated continental margin: Tectonics, v. 16, p. 290–304, doi: 10.1029/96TC03596.

Barth, A.P., Wooden, J.L., Howard, K.A., and Richards, J.L., 2008, Late Jurassic plutonism in the southwest U.S. Cordillera, *in* Wright, J.E., and Shervais, J.W., eds., Ophiolites, arcs and batholiths: A tribute to Cliff Hopson: Geological Society of America Special Paper 438, 379–396, doi: 10.1130/2008.2438(13).

Bartley, J.M., Coleman, D.S., and Glazner, A.F., 2008, Incremental pluton emplacement by magmatic crack-seal: Royal Society of Edinburgh Transactions, Earth and Environmental Science, v. 97, p. 383–396, doi: 10.1017/S0263593300001528.

Bateman, P.C., 1992, Plutonism in the central part of Sierra Nevada Batholith, California: U.S. Geological Survey Professional Paper 1483, 186 p.

Bateman, P.C., and Chappell, B.W., 1979, Crystallization, fractionation, and solidification of the Tuolumne Intrusive Series, Yosemite National Park, California: Geological Society of America Bulletin, v. 90, p. 465–482, doi: 10.1130/0016-7606(1979)90<465:CFASOT>2.0.CO;2.

Bejan, A., 1995, Convective heat transfer (second edition): New York, John Wiley & Sons, Inc., 652 p.

Bindeman, I.N., Fu, B., Kita, N.T., and Valley, J.W., 2008, Origin and evolution of silicic magmatism at Yellowstone based on ion microprobe analysis of isotopically zoned zircons: Journal of Petrology, v. 49, p. 163–193, doi: 10.1093/petrology/egm075.

Blake, S., and Fink, J.H., 2000, On the deformation and freezing of enclaves during magma mixing: Journal of Volcanology and Geothermal Research, v. 95, p. 1–8, doi: 10.1016/S0377-0273(99)00129-8.

Bracciali, L., Paterson, S.R., Memeti, V., and Rocchi, S., 2008, Build-up of the Tuolumne Batholith, California: The Johnson Granite Porphyry: LASI III Conference, Elba Island, abstracts, p. 17–18.

Brandon, M.T., Cowan, D.S., and Vance, J.A., 1988, The Late Cretaceous San Juan thrust system, San Juan Islands, Washington: Geological Society of America Special Paper 221, 81 p.

Brown, E.H., and Dragovich, J., 2003, Tectonic elements and evolution of northwest Washington: Washington Division of Geology and Earth Resources Geologic Map GM-52, scale 1:625,000.

Brown, E.H., and Gehrels, G., 2007, Detrital zircon constraints on terrane age and affinities and timing of orogenic events in the San Juan Islands and North Cascades, Washington: Canadian Journal of Earth Sciences, v. 44, p. 1375–1396, doi: 10.1139/E07-040.

Brown, E.H., and Walker, N.W., 1993, A magma-loading model for Barrovian metamorphism in the southeast Coast Plutonic Complex, British Columbia and Washington: Geological Society of America Bulletin, v. 105, p. 479–500, doi: 10.1130/0016-7606(1993)105<0479:AMLMFB>2.3.CO;2.

Brown, M., 2004, The mechanism of melt extraction from lower continental crust of orogens: Royal Society of Edinburgh Transactions, Earth Sciences, v. 95, p. 35–48, doi: 10.1017/S0263593300000900.

Brown, S.J.A., and Fletcher, I.R., 1999, SHRIMP U-Pb dating of the preeruption growth history of zircons from the 340 ka Whakamaru Ignimbrite, New Zealand: Evidence for >250 k.y. magma residence times: Geology, v. 27, p. 1035–1038, doi: 10.1130/0091-7613(1999)027<1035:SUPDOT>2.3.CO;2.

Burgess, S.D., and Miller, J.S., 2008, Construction, solidification, and internal differentiation of a large felsic arc pluton: Cathedral Peak granodiorite Sierra Nevada Batholith, *in* Annen, C., and Zellmer, G.F., eds., Dynamics of crustal magma transfer, storage and differentiation: Geological Society of London Special Publication 304, p. 203–233, doi: 10.1144/SP304.11.

Busby-Spera, C.J., 1988, Speculative tectonic model for the early Mesozoic arc of the southwest Cordilleran United States: Geology, v. 16, p. 1121–1125, doi: 10.1130/0091-7613(1988)016<1121:STMFTE>2.3.CO;2.

Carrigan, C.R., 1983, A heat pipe model for vertical, magma-filled conduits: Journal of Volcanology and Geothermal Research, v. 16, p. 279–298, doi: 10.1016/0377-0273(83)90034-3.

Carslaw, H.S., and Jaeger, J.C., 1959, Conduction of heat in solids (second edition): Oxford, UK, Clarendon Press, 510 p.

Castro, A., Martino, R., Vujovich, G., Otamendi, J., and Pinotti, L., D'eramo, F., Tibaldi, A., and Viñao, A., 2008, Top-down structures of mafic enclaves within the Valle Fértil magmatic complex (Early Ordovician, San Juan, Argentina): Geologica Acta, v. 6, p. 217–229.

Cater, F.W., 1982, Intrusive rocks of the Holden and Lucerne quadrangles, Washington—The relations of depth zones, composition, textures, and emplacement of plutons: U.S. Geological Survey Professional Paper 1220, 108 p.

Cater, F.W., and Crowder, D.F., 1967, Geologic map of the Holden Quadrangle, Snohomish and Chelan Counties, Washington: U.S. Geological Survey Map GQ-646, scale 1:62,500.

Charlier, B.L.A., Wilson, C.J.N., Lowenstern, J.B., Blake, S., van Calsteren, P.W., and Davidson, J.P., 2005, Magma generation at a large, hyperactive silicic volcano (Taupo, New Zealand) revealed by U/Th and U/Pb systematics in zircons: Journal of Petrology, v. 46, p. 3–32, doi: 10.1093/petrology/egh060.

Christensen, J.N., Halliday, A.N., Lee, D., and Hall, C.M., 1995, In situ Sr isotopic analysis by laser ablation: Earth and Planetary Science Letters, v. 136, p. 79–85, doi: 10.1016/0012-821X(95)00181-6.

Clarke, D.B., Henry, A.S., and White, M.A., 1998, Exploding xenoliths and the absence of "elephants' graveyards" in granite batholiths: Journal of Structural Geology, v. 20, p. 1325–1343, doi: 10.1016/S0191-8141(98)00082-0.

Clemens, J.D., 1998, Observations on the origins and ascent mechanisms of granitic magmas: Geological Society of London Journal, v. 155, p. 843–851, doi: 10.1144/gsjgs.155.5.0843.

Coleman, D.S., 2005, Field evidence for the assembly of the Half Dome pluton by amalgamation of small intrusions: Geological Society of America Abstracts with Programs, v. 37, no. 4, p. 71.

Coleman, D.S., and Glazner, A.F., 1997, The Sierra Crest magmatic event; rapid formation of juvenile crust during the Late Cretaceous in California: International Geology Review, v. 39, p. 768–787, doi: 10.1080/00206819709465302.

Coleman, D.S., Gray, W., and Glazner, A.F., 2004, Rethinking the emplacement and evolution of zoned plutons: Geochronologic evidence for incremental assembly of the Tuolumne Intrusive Suite, California: Geology, v. 32, p. 433–436, doi: 10.1130/G20220.1.

Coleman, D.S., Bartley, J.M., Glazner, A.F., and Law, R.D., 2005, Incremental assembly and emplacement of Mesozoic plutons in the Sierra Nevada and White and Inyo Ranges, California: Geological Society of America Field Forum Field Trip Guide (Rethinking the Assembly and Evolution of Plutons: Field Tests and Perspectives, 7–14 October 2005), 55 p., doi: 10.1130/2005.MCBFYT.FFG.

Costa, F., Chakraborty, S., and Dohmen, R., 2003, Diffusion coupling between trace and major elements and a model for calculation of magma residence times using plagioclase: Geochimica et Cosmochimica Acta, v. 67, p. 2189–2200, doi: 10.1016/S0016-7037(02)01345-5.

Crisp, J.A., 1984, Rates of magma emplacement and volcanic output: Journal of Volcanology and Geothermal Research, v. 20, p. 177–211, doi: 10.1016/0377-0273(84)90039-8.

Croft, D.R., and Lilley, D.G., 1977, Heat transfer calculations using finite-difference equations: London, Applied Science Publishers, Ltd., 283 p.

Davidson, J.P., Tepley, F.J., and Knesel, K.M., 1998, Isotopic fingerprinting may provide insights into evolution of magmatic systems: Eos (Transactions, American Geophysical Union), v. 79, p. 15, doi: 10.1029/98EO00135.

Davidson, J.P., Charlier, B.L.A., Hora, J.M., and Perlroth, R., 2005, Mineral isochrones and isotopic fingerprinting: Pitfalls and promises: Geology, v. 33, p. 29–32, doi: 10.1130/G21063.1.

Davidson, J.P., Morgan, D.J., Charlier, B.L.A., Harlou, R., and Hora, J.M., 2007, Microsampling and isotopic analysis of igneous rocks: Implications for the study of magmatic systems: Annual Review of Earth and Planetary Sciences, v. 35, p. 273–311, doi: 10.1146/annurev.earth.35.031306.140211.

Dawes, R.L., 1993, Mid-crustal, Late Cretaceous plutons of the North Cascades: Petrogenesis and implications for the growth of continental crust [Ph.D. thesis]: Seattle, University of Washington, 273 p.

DeBari, S.M., Miller, R.B., and Paterson, S.R., 1998, Genesis of tonalitic plutons in the Cretaceous magmatic arc of the North Cascades: Mixing of mantle derived magmas and melts of a garnet-bearing lower crust:

Geological Society of America Abstracts with Programs, v. 30, no. 7, p. A257–A258.
DeCelles, P.G., Ducea, M.N., Kapp, P., and Zandt, H.G., 2009, Cyclicity in Cordilleran orogenic systems: Nature Geoscience, v. 2, p. 251–257, doi: 10.1038/ngeo469.
de Silva, S.L., and Gosnold, W.A., 2007, Episodic construction of batholiths: Insights from the spatiotemporal development of an ignimbrite flare-up: Journal of Volcanology and Geothermal Research, v. 167, p. 320–335, doi: 10.1016/j.jvolgeores.2007.07.015.
Ducea, M., 2001, The California Arc: Thick granitic batholiths, eclogitic residues, lithospheric-scale thrusting, and magmatic flare-ups: GSA Today, v. 11, p. 4–10, doi: 10.1130/1052-5173(2001)011<0004:TCATGB>2.0.CO;2.
Ducea, M.N., 2002, Constraints on the bulk compositions and root foundering rates of continental arcs: A California perspective: Journal of Geophysical Research, v. 107, 2304, doi: 10.1029/2001JB000643.
Ducea, M.N., and Barton, M.D., 2007, Igniting flare-up events in Cordilleran arcs: Geology, v. 35, p. 1047–1050, doi: 10.1130/G23898A.1.
Dunne, C.G., Garvey, T.P., Osborne, M., Schneidereit, D., Fritsche, A.E., and Walker, J.D., 1998, Geology of the Inyo Mountains Volcanic Complex: Implications for Jurassic paleogeography of the Sierran magmatic arc in eastern California: Geological Society of America Bulletin, v. 110, p. 1376–1397, doi: 10.1130/0016-7606(1998)110<1376:GOTIMV>2.3.CO;2.
Economos, R., 2009, Vertical changes in magmatic architecture, hybridization and geochemistry in a tilted arc crustal section of the Gobi-Tienshan intrusive complex, Mongolia [Ph.D. thesis]: Los Angeles, University of Southern California, AAT 3368519, 272 p.
Economos, R., Memeti, V., Paterson, S.R., Miller, J., Erdmann, S., and Žák, J., 2010, Causes of compositional diversity in a lobe of the Half Dome granodiorite, Tuolumne batholith, central Sierra Nevada, CA: Royal Society of Edinburgh Transactions, Earth and Environmental Science, v. 100, p. 173–183, doi: 10.1017/S1755691009016065.
Erikson, E.H., 1977, Petrology and petrogenesis of the Mount Stuart batholith—Plutonic equivalent of the high-alumina basalt association?: Contributions to Mineralogy and Petrology, v. 60, p. 183–207, doi: 10.1007/BF00372281.
Evans, B.W., and Davidson, G.F., 1999, Kinetic control of metamorphic imprint during synplutonic loading of batholiths: An example from Mount Stuart, Washington: Geology, v. 27, p. 415–418, doi: 10.1130/0091-7613(1999)027<0415:KCOMID>2.3.CO;2.
Farris, D.W., and Paterson, S.R., 2007, Physical contamination of silicic magmas and fractal fragmentation of xenoliths in Paleocene plutons on Kodiak Island, AK: Canadian Mineralogist, v. 45, p. 107–129, doi: 10.2113/gscanmin.45.1.107.
Francis, P., and Rundle, C.C., 1976, Rates of production of the main magma types in the central Andes: Geological Society of America Bulletin, v. 87, p. 474–480, doi: 10.1130/0016-7606(1976)87<474:ROPOTM>2.0.CO;2.
Furlong, K.P., and Myers, J.D., 1985, Thermal-mechanical modeling of the role of thermal stresses and stoping in magma contamination: Journal of Volcanology and Geothermal Research, v. 24, p. 179–191, doi: 10.1016/0377-0273(85)90032-0.
Furlong, K.P., and Shive, P.N., 1983, Determination of timing of volcanic events by secular variation and thermal modeling: Geophysical Research Letters, v. 10, p. 701–704, doi: 10.1029/GL010i008p00701.
Furlong, K.P., Hanson, R.B., and Bowers, J.R., 1991, Modeling thermal regimes, *in* Kerrick, D.M., ed., Contact metamorphism: Mineralogical Society of America Reviews in Mineralogy, v. 26, p. 437–498.
Gagnevin, D., Daly, J.S., Poli, G., and Morgan, D., 2005, Microchemical and Sr isotopic investigation of zoned K-feldspar megacrysts: Insights into the petrogenesis of a granitic system and disequilibrium crystal growth: Journal of Petrology, v. 46, p. 1689–1724, doi: 10.1093/petrology/egi031.
Gamble, J.A., Price, R.C., Smith, I.E.M., McIntosh, W.C., and Dunbar, N.W., 2003, $^{40}Ar/^{39}Ar$ geochronology of magmatic activity, magma flux and hazards at Ruapehu volcano, Taupo Volcanic Zone, New Zealand: Journal of Volcanology and Geothermal Research, v. 120, p. 271–287, doi: 10.1016/S0377-0273(02)00407-9.
Gehrels, G.E., and 16 others, 2009, U-Th-Pb geochronology of the Coast Mountains Batholith in north-coastal British Columbia: Constraints on age, petrogenesis, and tectonic evolution: Geological Society of America Bulletin, v. 121, p. 1341–1361, doi: 10.1130/B26404.1.
Glazner, A.F., Bartley, J.M., Coleman, D.S., Gray, W., and Taylor, R.Z., 2004, Are plutons assembled over millions of years by amalgamation from small magma chambers?: GSA Today, v. 14, p. 4–11, doi: 10.1130/1052-5173(2004)014<0004:APAOMO>2.0.CO;2.
Gray, W., 2003, Chemical and thermal evolution of the Late Cretaceous Tuolumne Batholith, Yosemite National Park, California [Ph.D. thesis]: Chapel Hill, University of North Carolina, 202 p.
Gray, W., Glazner, A.F., Coleman, D.S., and Bartley, J.M., 2008, Long-term geochemical variability of the Late Cretaceous Tuolumne Intrusive Suite, central Sierra Nevada, California: Geological Society of London Journal, v. 304, p. 183–201, doi: 10.1144/SP304.10.
Guillou-Frottier, L., Burov, E.B., and Milesi, J.P., 2000, Genetic links between ash-flow calderas and associated ore deposits as revealed by large-scale thermo-mechanical modeling: Journal of Volcanology and Geothermal Research, v. 102, p. 339–361, doi: 10.1016/S0377-0273(00)00246-8.
Hanson, R.B., and Barton, M.D., 1989, Thermal development of low-pressure metamorphic belts; results from two-dimensional numerical models: Journal of Geophysical Research, v. 94, p. 10,363–10,377, doi: 10.1029/JB094iB08p10363.
Hanson, R.B., and Glazner, A.F., 1995, Thermal requirements for extensional emplacement of granitoids: Geology, v. 23, p. 213–216, doi: 10.1130/0091-7613(1995)023<0213:TRFEEO>2.3.CO;2.
Hanson, R.B., Sorensen, S.S., Barton, M.D., and Fiske, R.S., 1993, Long-term evolution of fluid-rock interactions in magmatic arcs; evidence from the Ritter Range pendant, Sierra Nevada, California, and numerical modeling: Journal of Petrology, v. 34, p. 23–62, doi: 10.1093/petrology/34.1.23.
Hardee, H.C., 1982, Incipient magma chamber formation as a result of repetitive intrusions: Bulletin of Volcanology, v. 45, p. 41–49, doi: 10.1007/BF02600388.
Haugerud, R.A., van der Heyden, P., Tabor, R.W., Stacey, J.S., and Zartman, R.E., 1991, Late Cretaceous and early Tertiary plutonism and deformation in the Skagit Gneiss Complex, North Cascade Range, Washington and British Columbia: Geological Society of America Bulletin, v. 103, p. 1297–1307, doi: 10.1130/0016-7606(1991)103<1297:LCAETP>2.3.CO;2.
Hora, J.M., Singer, B.S., and Worner, G., 2007, Volcano evolution and eruptive flux on the thick crust of the Andean Central Volcanic Zone: $^{40}Ar/^{39}Ar$ constraints from Volcán Parinacota, Chile: Geological Society of America Bulletin, v. 119, p. 343–362, doi: 10.1130/B25954.1.
Hoskin, P.W.O., Kinny, P.D., and Wyborn, D., 1998, Chemistry of hydrothermal zircon: Investigating timing and nature of water-rock interaction, *in* Arehart, G.B., and Hulston, J.R., eds., Water-rock interaction: Rotterdam, Balkema, p. 545–548.
Huber, N.K., Bateman, P.C., and Wahrhaftig, C., 1989, Geologic map of Yosemite National Park and vicinity, California: U.S. Geological Survey Miscellaneous Investigations Series Map I-1874, scale 1:125,000.
Hurlow, H.A., 1992, Structural and U-Pb geochronologic studies of the Pasayten fault, Okanogan Range batholith, and southeastern Cascades crystalline core, Washington [Ph.D. thesis]: Seattle, University of Washington, 168 p.
Hutton, D.H.W., 1982, A tectonic model for the emplacement of the Main Donegal granite, NW Ireland: Geological Society of London Journal, v. 139, p. 615–631, doi: 10.1144/gsjgs.139.5.0615.
Hutton, D.H.W., 1992, Granite sheeted complexes: Evidence for the dyking ascent mechanism: Royal Society of Edinburgh Transactions, Earth Sciences, v. 83, p. 377–382.
Jaeger, J.C., 1961, The cooling of irregularly shaped igneous bodies: American Journal of Science, v. 259, p. 721–734, doi: 10.2475/ajs.259.10.721.
Johnson, S.E., Paterson, S.R., and Tate, M.C., 1999, Structure and emplacement history of multiple-center, cone-sheet-bearing ring complex: The Zarza Intrusive Complex, Baja California, Mexico: Geological Society of America Bulletin, v. 111, p. 607–619, doi: 10.1130/0016-7606(1999)111<0607:SAEHOA>2.3.CO;2.
Journeay, J.M., and Friedman, R.M., 1993, The Coast Belt thrust system: Evidence of Late Cretaceous shortening in southwest British Columbia: Tectonics, v. 12, p. 756–775, doi: 10.1029/92TC02773.
Kistler, R.W., and Fleck, R.J., 1994, Field guide for a transect of the Central Sierra Nevada, California: Geochronology and isotope geology: U.S. Geological Survey Open-File Report 94-267, 53 p.
Kistler, R.W., Chappell, B.W., Peck, D.L., and Bateman, P.C., 1986, Isotopic variation in the Tuolumne Intrusive Suite, central Sierra Nevada, California: Contributions to Mineralogy and Petrology, v. 94, p. 205–220, doi: 10.1007/BF00592937.
Koyaguchi, T., and Kaneko, K., 1999, A two-stage thermal evolution model of magmas in continental crust: Journal of Petrology, v. 40, p. 241–254, doi: 10.1093/petrology/40.2.241.
Kuritani, T., 1999, Thermal and compositional evolution of a cooling magma chamber boundary layer fractionation; model and its application for primary magma estimation: Geophysical Research Letters, v. 26, p. 2029–2032, doi: 10.1029/1999GL900381.
Lackey, J.S., Valeey, J.W., Chen, J.H., and Stockli, D., 2008, Dynamic magma systems, crustal recycling, and alteration in the Central Sierra Nevada Batholith: The oxygen isotope record: Journal of Petrology, v. 49, p. 1397–1426, doi: 10.1093/petrology/egn030.
Lagarde, J.L., Brun, J.P., and Gapais, D., 1990, Formation of epizonal granitic plutons by in situ assemblage of laterally expanding magma: Paris, Académie des Sciences Comptes Rendus, v. 310, p. 1109–1114.
Lipman, P.W., 2007, Incremental assembly and prolonged consolidation of Cordilleran magma chambers: Evidence from the Southern Rocky Mountain volcanic field: Geosphere, v. 3, p. 42–70, doi: 10.1130/GES00061.1.
Liu, M., and Furlong, K.P., 1992, Cenozoic volcanism in the California Coast Ranges: Numerical solutions: Journal of Geophysical Research, v. 97, p. 4941–4951, doi: 10.1029/92JB00193.
MacDonald, J.H., Harper, G.D., Miller, R.B., Miller, J.S., Mlinarevic, A.N., and Schultz, C., 2008, Geochemistry of the polygenetic Ingalls ophiolite complex, central Cascades, Washington: Geochemistry, tectonic setting, and regional correlations, *in* Wright, J.E., and Shervais, J.W., eds., Ophiolites, arcs, and batholiths: A tribute to Cliff Hopson: Geological Society of America Special Paper 438, p. 133–159, doi: 10.1130/2008.2438(04).
Magloughlin, J.F., 1993, A Nason terrane trilogy: I, Nature and significance of pseudotachylyte: II, Summary of the structural and tectonic history: III, Major and trace element geochemistry and strontium and neodymium isotope geochemistry of the Chiwaukum Schist, amphibolite, and meta-tonalite gneiss of the Nason terrane [Ph.D. thesis]: Minneapolis, University of Minnesota, 325 p.
Marsh, B.D., 1982, On the mechanics of igneous diapirism, stoping, and zone melting: American Journal of Science, v. 282, p. 808–855, doi: 10.2475/ajs.282.6.808.
Marsh, B.D., 1996, Solidification fronts and magmatic evolution: Mineralogical Magazine, v. 60, p. 5–40, doi: 10.1180/minmag.1996.060.398.03.
Mattinson, J.M., 2005, Zircon U-Pb chemical abrasion ("CA-TIMS") method: Combined annealing and multi-step partial dissolution analysis for improved precision and accuracy of zircon ages: Chemical Geology, v. 220, p. 47–66, doi: 10.1016/j.chemgeo.2005.03.011.
Matzel, J.P., 2004, Rates of tectonic and magmatic processes in the North Cascades continental magmatic arc [Ph.D.

thesis]: Cambridge, Massachusetts Institute of Technology, 249 p.

Matzel, J.P., Bowring, S.A., and Miller, R.B., 2004, Protolith age of the Swakane Gneiss, North Cascades, Washington: Evidence of rapid underthrusting of sediments beneath an arc: Tectonics, v. 23, TC6009, doi: 10.1029/2003TC001577.

Matzel, J., Mundil, R., Paterson, S., Renne, P., and Nomade, S., 2005, Evaluating pluton growth models using high resolution geochronology: Tuolumne Intrusive Suite, Sierra Nevada, CA: Geological Society of America Abstracts with Programs, v. 37, no. 7, p. 131.

Matzel, J.E.P., Bowring, S.A., and Miller, R.B., 2006a, Time scales of pluton construction at differing crustal levels: Examples from the Mount Stuart and Tenpeak intrusions, North Cascades, Washington: Geological Society of America Bulletin, v. 118, p. 1412–1430, doi: 10.1130/B25923.1.

Matzel, J., Miller, J.S., Mundil, R., and Paterson, S.R., 2006b, Zircon saturation and the growth of the Cathedral Peak pluton, CA: Geochimica et Cosmochimica Acta, v. 70, p. A403, doi: 10.1016/j.gca.2006.06.813.

Matzel, J.P., Bowring, S.A., and Miller, R.B., 2008, Spatial and temporal variations in Nd isotopic signatures across the crystalline core of the North Cascades, Washington, *in* Wright, J.E., and Shervais, J.W., eds., Ophiolites, arcs, and batholiths: A tribute to Cliff Hopson: Geological Society of America Special Paper 438, p. 499–516, doi: 10.1130/2008.2438(18).

McLeod, P., and Sparks, R.S.J., 1998, The dynamics of xenolith assimilation: Contributions to Mineralogy and Petrology, v. 132, p. 21–33, doi: 10.1007/s004100050402.

McNulty, B.A., Tong, W., and Tobisch, O.T., 1996, Assembly of a dike-fed magma chamber: The Jackass Lakes pluton, central Sierra Nevada, California: Geological Society of America Bulletin, v. 108, p. 926–940, doi: 10.1130/0016-7606(1996)108<0926:AOADFM>2.3.CO;2.

Memeti, V., and Paterson, S.R., 2008, Heterogeneous Kfs megacryst size and abundance variation in the northern Cathedral Peak lobe, Tuolumne batholith: Geological Society of America Abstracts with Programs, v. 40, no. 1, p. 74.

Memeti, V., Gehrels, G., Paterson, S., and Thompson, J., 2007, Miogeoclinal strata in high Sierra Nevada pendants: Detrital zircon ages reveal additional evidence for a Cretaceous "Mojave-Snow Lake fault" (MSLF): Geological Society of America Abstracts with Programs, v. 39, no. 6, p. 279.

Memeti, V., Krause, J., Anderson, J.L., and Paterson, S.R., 2009, Interpreting Al-in Hornblende and Hbl-Plag thermobarometry results from the Tuolumne batholith and magmatic lobes in conjunction with single mineral element distribution electron microprobe maps: Eos (Transactions, American Geophysical Union), v. 90, no. 52, fall meeting supplement, abs. V42A-06.

Memeti, V., Paterson, S., Matzel, J., Mundil, R., and Okaya, D., 2010, Using magmatic lobes as "snapshots" of magma chamber growth to help decipher the growth and evolution of large, composite batholiths: An example from the Tuolumne Intrusion, Sierra Nevada, CA: Geological Society of America Bulletin, v. 122, p. 1912–1931, doi: 10.1130/B30004.1.

Miller, J., Miller, R., Wooden, J., and Miller, B., 2003, A complex magmatic injection zone in the Half Dome Granodiorite, Tuolumne Intrusive Suite, Sierra Nevada Batholith, CA: Geological Society of America Abstracts with Programs, v. 35, no. 4, p. 18.

Miller, J.S., Matzel, J.E., Miller, C.F., Burgess, S.D., and Miller, R.B., 2007, Zircon growth and recycling during the assembly of large, composite arc plutons: Journal of Volcanology and Geothermal Research, v. 167, p. 282–299, doi: 10.1016/j.jvolgeores.2007.04.019.

Miller, J.S., Barth, A., Matzel, J., Wooden, J., and Burgess, S., 2008, Zircon recycling in arc intrusions: Eos (Transactions, American Geophysical Union), v. 89, no. 53, fall meeting supplement, abs. V43J-08.

Miller, R.B., 1985, The ophiolitic Ingalls Complex, North Cascades, Washington: Geological Society of America Bulletin, v. 96, p. 27–42, doi: 10.1130/0016-7606(1985)96<27:TOICNC>2.0.CO;2.

Miller, R.B., and Bowring, S.A., 1990, Structure and chronology of the Oval Peak batholith and adjacent rocks: Implications for the Ross Lake fault zone, North Cascades, Washington: Geological Society of America Bulletin, v. 102, p. 1361–1377, doi: 10.1130/0016-7606(1990)102<1361:SACOTO>2.3.CO;2.

Miller, R.B., and Mogk, D.W., 1987, Ultramafic rocks of a fracture-zone ophiolite, North Cascades, Washington: Tectonophysics, v. 142, p. 261–289, doi: 10.1016/0040-1951(87)90127-2.

Miller, R.B., and Paterson, S.R., 1999, In defense of magmatic diapirs: Journal of Structural Geology, v. 21, p. 1161–1173, doi: 10.1016/S0191-8141(99)00033-4.

Miller, R.B., and Paterson, S.R., 2001a, Construction of mid-crustal sheeted plutons: Examples from the North Cascades, Washington: Geological Society of America Bulletin, v. 113, p. 1423–1442, doi: 10.1130/0016-7606(2001)113<1423:COMCSP>2.0.CO;2.

Miller, R.B., and Paterson, S.R., 2001b, Influence of lithological heterogeneity, mechanical anisotropy, and magmatism on the rheology of an arc, North Cascades, Washington: Tectonophysics, v. 342, p. 351–370, doi: 10.1016/S0040-1951(01)00170-6.

Miller, R.B., and Snoke, A.W., eds., 2009, Crustal cross sections from the western North American Cordillera and elsewhere: Implications for tectonic and petrologic processes: Geological Society of America Special Paper 456, 286 p., doi: 10.1130/2009.2456.

Miller, R.B., Paterson, S.R., DeBari, S.M., and Whitney, D.L., 2000, North Cascades Cretaceous crustal section: Changing kinematics, rheology, metamorphism, pluton emplacement and petrogenesis from 0 to 40 km depth, *in* Woodsworth, G.J., et al., eds., Guidebook for geological field trips in southwestern British Columbia and northern Washington: Geological Society of America Cordilleran Section Annual Meeting: Vancouver, Geological Association of Canada, p. 229–278.

Miller, R.B., Paterson, S.R., Lebit, H., Alsleben, H., and Luneburg, C., 2006, Significance of composite lineations in the mid- to deep crust: A case study from the North Cascades, Washington: Journal of Structural Geology, v. 28, p. 302–322, doi: 10.1016/j.jsg.2005.11.003.

Miller, R.B., Paterson, S.R., and Matzel, J.P., 2009, Plutonism at different crustal levels: Insights from the ~5–40 km (paleodepth) North Cascades crustal section, Washington, *in* Miller, R.B., and Snoke, A.W., eds., Crustal cross sections from the western North American Cordillera and elsewhere: Implications for tectonic and petrologic processes: Geological Society of America Special Paper 456, p. 125–149, doi: 10.1130/2009.2456(05).

Misch, P., 1966, Tectonic evolution of the northern Cascades of Washington State—A west Cordilleran case history: Canadian Institute of Mining and Metallurgy Special Volume 8, p. 101–148.

Morgan, D.J., Jerram, D.A., Chertkoff, D.G., Davidson, J.P., Pearson, D.G., Kronz, A., and Nowell, G.M., 2007, Combining CSD and isotopic microanalysis: Magma supply and mixing processes at Stromboli volcano, Aeolian Islands, Italy: Earth and Planetary Science Letters, v. 260, p. 419–431, doi: 10.1016/j.epsl.2007.05.037.

Mundil, R., Nomade, S., Paterson, S., and Renne, P.R., 2004, Geochronological constraints ($^{40}Ar/^{39}Ar$ and U/Pb) on the thermal history of the Tuolumne Intrusive Suite (Sierra Nevada, California): Eos (Transactions, American Geophysical Union) fall meeting supplement, v. 85, p. 47.

Needy, S.K., Anderson, J.L., Wooden, J.L., Barth, A.P., Paterson, S.R., Memeti, V., and Pignotta, G.S., 2009, Mesozoic magmatism in an upper- to middle-crustal section through the Cordilleran continental margin arc, eastern Transverse Ranges, California, *in* Miller, R.B., and Snoke, A.W., eds., Crustal cross sections from the western North America Cordillera and elsewhere: Implications for tectonic and petrologic processes: Geological Society of America Special Paper 456, p. 187–218, doi: 10.1130/2009.2456(07).

Oliver, H.W., Moore, J.G., and Sikora, R.F., 1988, Internal structure and vertical extent of the Sierra Nevada batholith, California, from specific-gravity and gravity data, *in* Guangzhi, T., et al., eds., Petrogenesis and mineralization of granitoids—Proceedings of 1987 Guangzhou International Symposium: Beijing, Chinese Scientific Book Service, 1224 p.

Parsons, T., Sleep, N.H., and Thompson, G.A., 1992, Host rock rheology controls on the emplacement of tabular intrusions; implications for underplating of extending crust: Tectonics, v. 11, p. 1348–1356, doi: 10.1029/92TC01105.

Paterson, S.R., 2009, Magmatic tubes, troughs, pipes, and diapirs: Late-stage convective instabilities resulting in complex permeable networks in crystal-rich magmas of the Tuolumne Batholith, Sierra Nevada, California: Geosphere, v. 5, p. 496–527, doi: 10.1130/GES00214.1.

Paterson, S.R., and Farris, D.W., 2008, Downward host rock transport and the formation of rim monoclines during the emplacement of Cordilleran batholiths: Royal Society of Edinburgh Transactions, Earth and Environmental Science, v. 97, p. 397–413, doi: 10.1017/S026359330000153X.

Paterson, S.R., and Miller, R.B., 1998, Mid-crustal magmatic sheets in the Cascades Mountains, Washington: Implications for magma ascent: Journal of Structural Geology, v. 20, p. 1345–1363, doi: 10.1016/S0191-8141(98)00072-8.

Paterson, S.R., and Vernon, R.H., 1995, Bursting the bubble of ballooning plutons: A return to nested diapirs emplaced by multiple processes: Geological Society of America Bulletin, v. 107, p. 1356–1380, doi: 10.1130/0016-7606(1995)107<1356:BTBOBP>2.3.CO;2.

Paterson, S.R., Miller, R.B., Anderson, J.L., Lund, S.P., Bendixen, J., Taylor, N., and Fink, T., 1994, Emplacement and evolution of the Mount Stuart batholith, *in* Swanson, D.A., and Haugerud, R.A., eds., Geologic field trips in the Pacific Northwest: Geological Society of America Annual Meeting Field Trip Guidebook, v. 2F, p. 1–47.

Paterson, S.R., Matzel, J.P., and Miller, R.B., 2002, Spatial and temporal evolution of magmatic systems in a continental margin arc: The Cascades core, Washington: Geological Society of America Abstracts with Programs, v. 34, n. 5, p. A-96.

Paterson, S.R., Miller, R.B., Alsleben, H., Whitney, D.L., Valley, P.M., and Hurlow, H., 2004, Driving mechanisms for >40 km of exhumation during contraction and extension in a continental arc, Cascades core, Washington: Tectonics, v. 23, TC3005, doi: 10.1029/2002TC001440.

Paterson, S., Okaya, D., Matzel, J., Memeti, V., and Mundil, R., 2007, Size and longevity of magma chambers in the Tuolumne batholith: A comparison of thermal modeling and cooling thermochronology: Eos (Transactions, American Geophysical Union), v. 88, p. 52.

Paterson, S.R., Žák, J., and Janoušek, V., 2008, Growth of complex magmatic zones during recycling of older magmatic phases: The Sawmill Canyon area in the Tuolumne Batholith, Sierra Nevada, California: Journal of Volcanology and Geothermal Research, v. 177, p. 457–484, doi: 10.1016/j.jvolgeores.2008.06.024.

Paterson, S., Okaya, D., Matzel, J., Memeti, V., and Mundil, R., 2009, Thermal models, stable isotopes and cooling ages from the incrementally constructed Tuolumne batholith, Sierra Nevada: Why large chambers did exist: Eos (Transactions, American Geophysical Union), Fall Meeting Supplement, abs. T24C-04.

Peacock, S.M., Rushmer, T., and Thompson, A.B., 1994, Partial melting of subducting oceanic crust: Earth and Planetary Science Letters, v. 121, p. 227–244, doi: 10.1016/0012-821X(94)90042-6.

Petford, N., Lister, J.R., and Kerr, R.C., 1994, The ascent of felsic magmas in dykes: Lithos, v. 32, p. 161–168, doi: 10.1016/0024-4937(94)90028-0.

Pignotta, G.S., Paterson, S.R., and Okaya, D., 2001a, Cracking the stoping paradigm: Field and modeling constraints from the Sierra Nevada batholith: Eos (Transactions, American Geophysical Union), v. 82, p. 47.

Pignotta, G.S., Paterson, S.R., and Pettersson, D., 2001b, Voluminous stoping in the Mitchell Peak Granodiorite, Sierra Nevada, California: Geological Society of America, Cordilleran Section, 97th annual meeting

and American Association of Petroleum Geologists, Pacific Section, annual meeting, session 33.
Pitcher, W.S., and Berger, A.R., 1972, The geology of Donegal: A study of granite emplacement and unroofing: New York, Wiley, 435 p.
Plummer, C.C., 1980, Dynamothermal contact metamorphism superimposed on regional metamorphism of pelitic rocks of the Chiwaukum Mountains area, Washington Cascades: Summary: Geological Society of America Bulletin, v. 91, p. 386–388, doi: 10.1130/0016-7606(1980)91<386:DCMSOR>2.0.CO;2.
Ramos, F.C., and Reid, M.R., 2005, Distinguishing melting of heterogeneous mantle sources from crustal contamination: Insights from Sr isotopes at the phenocryst scale, Pisgah Crater, California: Journal of Petrology, v. 46, p. 999–1012, doi: 10.1093/petrology/egi008.
Rubin, C.M., Saleeby, J.B., Cowan, D.S., Brandon, M.T., and McGroder, M.F., 1990, Regionally extensive mid-Cretaceous west-vergent thrust system in the northwestern Cordillera: Implications for continent-margin tectonism: Geology, v. 18, p. 276–280, doi: 10.1130/0091-7613(1990)018<0276:REMCWV>2.3.CO;2.
Saleeby, J.B., 1990, Progress in tectonic and petrogenetic studies in an exposed cross-section of young (c. 100 Ma) continental crust, southern Sierra Nevada, California, *in* Salisbury, M.H., and Fountain, D.M., eds., Exposed cross-sections of the continental crust: Norwell, Massachusetts, Kluwer, p. 137–159.
Saleeby, J., Ducea, M., and Clemens-Knott, D., 2003, Production and loss of high-density batholithic root, southern Sierra Nevada region: Tectonics, v. 22, p. 6, doi: 10.1029/2002TC001374.
Saleeby, J.B., Ducea, M.N., Busby, C.J., Nadin, E.S., and Wetmore, P.H., 2008, Chronology of pluton emplacement and regional deformation in the southern Sierra Nevada batholith, California, *in* Wright, J.E., and Shervais, J.W., eds., Ophiolites, arcs and batholiths: A tribute to Cliff Hopson: Geological Society of America Special Paper 438, p. 397–427, doi: 10.1130/2008.2438(14).
Scandone, R., Cashman, K.V., and Malone, S.D., 2007, Magma supply, magma ascent and the style of volcanic eruptions: Earth and Planetary Science Letters, v. 253, p. 513–529, doi: 10.1016/j.epsl.2006.11.016.
Sleep, N.H., 1975, Formation of oceanic crust: Some thermal constraints: Journal of Geophysical Research, v. 80, p. 4037–4042, doi: 10.1029/JB080i029p04037.
Sleep, N.H., 1991, Hydrothermal circulation, anhydrite precipitation, and thermal structure at ridge axes: Journal of Geophysical Research, v. 96, p. 2375–2387, doi: 10.1029/90JB02335.
Solgadi, F., and Sawyer, E.W., 2008, Formation of igneous layering in granodiorite by gravity flow: A field, microstructure and geochemical study of the Tuolumne Intrusive Suite at Sawmill Canyon, California: Journal of Petrology, v. 49, p. 2009–2042, doi: 10.1093/petrology/egn056.
Sparks, R.S.J., and Marshall, L.A., 1986, Thermal and mechanical constraints on mixing between mafic and silicic magmas: Journal of Volcanology and Geothermal Research, v. 29, p. 99–124, doi: 10.1016/0377-0273(86)90041-7.
Stephens, W.E., 1992, Spatial, compositional, and rheological constraints on the origin of zoning in the Criffell pluton, Scotland: Royal Society of Edinburgh Transactions, Earth Sciences, v. 83, p. 191–199.
Tabor, R.W., Frizzell, V.A., Jr., Whetten, J.T., Waitt, R.B., Jr., Swanson, D.A., Byerly, G.R., Booth, D.B., Hetherington, M.J., and Zartman, R.E., 1987, Geologic map of the Chelan 30′ by 60′ Quadrangle, Washington: U.S. Geological Survey Geologic Investigations Series I-1661, scale 1:100,000.
Tabor, R.W., Haugerud, R.A., and Miller, R.B., 1989, Overview of the geology of the North Cascades: American Geophysical Union, International Geological Congress Trip T307, 62 p.
Tabor, R.W., Frizzell, V.A., Booth, D.B., Waitt, R.B., Whetten, J.T., and Zartman, R.E., 1993, Geologic map of the Skykomish River 30- by 60-minute quadrangle, Washington: U.S. Geological Survey Map I-1963, scale 1:100,000.
Tikoff, B., and Teyssier, C., 1994, Strain modeling of displacement-field partitioning in transpressional orogens: Journal of Structural Geology, v. 16, p. 1575–1588, doi: 10.1016/0191-8141(94)90034-5.
Titus, S.J., Clark, R., and Tikoff, B., 2005, Geologic and geophysical investigation of two fine-grained granites, Sierra Nevada Batholith, California: Evidence for structural controls on emplacement and volcanism: Geological Society of America Bulletin, v. 117, p. 1256–1271, doi: 10.1130/B25689.1.
Tobisch, O.T., Saleeby, J.B., and Fiske, F.S., 1986, Structural history of continental volcanic arc rocks, eastern Sierra Nevada, California: A case for extensional tectonics: Tectonics, v. 5, p. 65–94, doi: 10.1029/TC005i001p00065.
Valley, P.M., Whitney, D.L., Paterson, S.R., Miller, R.B., and Alsleben, H., 2003, Metamorphism of the deepest exposed arc rocks in the Cretaceous to Paleogene Cascades belt, Washington: Evidence for large-scale vertical motion in a continental arc: Journal of Metamorphic Geology, v. 21, p. 203–220, doi: 10.1046/j.1525-1314.2003.00437.x.
Vernon, R.H., and Paterson, S.R., 2007, Mesoscopic structures resulting from crystal accumulation and melt movement in granites: Royal Society of Edinburgh Transactions, Earth and Environmental Science, v. 97, p. 369–381, doi: 10.1017/S0263593300001516.
Vigneresse, J.L., and Bouchez, J.L., 1997, Successive granitic magma batches during pluton emplacement: The case study of Cabeza de Araya, Spain: Journal of Petrology, v. 38, p. 1767–1776, doi: 10.1093/petrology/38.12.1767.
Wadge, G., 1981, The variation of magma discharge during basaltic eruptions: Journal of Volcanology and Geothermal Research, v. 11, p. 139–168, doi: 10.1016/0377-0273(81)90020-2.
Walker, B.A., Jr., Miller, C.F., Lowery Claiborne, L., Wooden, J.L., and Miller, J.S., 2007, Geology and geochronology of the Spirit Mountain batholith, southern Nevada: Implications for timescales and physical processes of batholith construction: Journal of Volcanology and Geothermal Research, v. 167, p. 239–262, doi: 10.1016/j.jvolgeores.2006.12.008.
Wallace, G.S., and Bergantz, G.W., 2005, Reconciling heterogeneity in crystal zoning data: An application of shared characteristic diagrams at Chaos Crags, Lassen Volcanic Center, California: Contributions to Mineralogy and Petrology, v. 149, p. 98–112, doi: 10.1007/s00410-004-0639-2.
Weinberg, R.F., 1999, Mesoscale pervasive felsic magma migration: Alternatives to dyking: Lithos, v. 46, p. 393–410, doi: 10.1016/S0024-4937(98)00075-9.
Whitney, D.L., Miller, R.B., and Paterson, S.R., 1999, P-T-t constraints on mechanisms of vertical tectonic motion in a contractional orogen: Journal of Metamorphic Geology, v. 17, p. 75–90, doi: 10.1046/j.1525-1314.1999.00181.x.
Whittington, A.G., Hofmeister, A.M., and Nabelek, P.I., 2009, Temperature-dependent thermal diffusivity of the Earth's crust and implications for magmatism: Nature, v. 458, p. 319–321, doi: 10.1038/nature07818.
Wiebe, R.A., and Collins, W.J., 1998, Depositional features and stratigraphic sections in granitic plutons: Implications for the emplacement and crystallization of granitic magma: Journal of Structural Geology, v. 20, p. 1273–1289, doi: 10.1016/S0191-8141(98)00059-5.
Wilson, D.S., Clague, D.A., Sleep, N.H., and Morton, J.L., 1988, Implications of magma convection for the size and temperature of magma chambers at fast spreading ridges: Journal of Geophysical Research, v. 93, p. 11,974–11,984, doi: 10.1029/JB093iB10p11974.
Yoshinobu, A.S., Okaya, D.A., and Paterson, S.R., 1998, Modelling the thermal evolution of fault-controlled magma emplacement models: Journal of Structural Geology, v. 20, p. 1205–1218, doi: 10.1016/S0191-8141(98)00064-9.
Žák, J., and Paterson, S.R., 2005, Characteristics of internal contacts in the Tuolumne Batholith, central Sierra Nevada, California (USA): Implications for episodic emplacement and physical processes in a continental arc magma chamber: Geological Society of America Bulletin, v. 117, p. 1242–1255, doi: 10.1130/B25558.1.
Žák, J., Paterson, S.R., and Memeti, V., 2007, Four magmatic fabrics in the Tuolumne batholith, central Sierra Nevada, California (USA): Implications for interpreting fabric patterns in plutons and evolution of magma chambers in the upper crust: Geological Society of America Bulletin, v. 119, p. 184–201, doi: 10.1130/B25773
Žák, J., Paterson, S.R., Kabele, P., and Janousek, V., 2009, The Mammoth Peak sheeted complex, Tuolumne Batholith, central Sierra Nevada, California: A record of initial growth or late thermal contraction in a magma chamber?: Contributions to Mineralogy and Petrology, v. 158, p. 447–470, doi: 10.1007/s00410-009-0391-8.

Manuscript Received 26 March 2011
Revised Manuscript Received 11 August 2011
Manuscript Accepted 18 August 2011